Reproducibility in simulation-based prediction of natural knee mechanics

M&S processes specification documents

DU02 from Natural Knee Data, University of Denver

Hospital for Special Surgery

Metadata

Contributors:

- Carl Imhauser, PhD

- Shady Elmasry, PhD

Contacts:

1- Carl Imhauser

imhauserc@hss.edu
+1 (212) 606-1079
510 East 73rd Street,
New York, NY 10021

2- Shady Elmasry

elmasrys@hss.edu
+1 (212) 774-7275
510 East 73rd Street,
New York, NY 10021

Corresponding Author:

Carl Imhauser, PhD

Date: 09/04/2018

Table of Contents

List of acronyms

ACL	Anterior Cruciate Ligament
AM	Anteromedial
AL	Anterolateral
PL	Posterolateral
PCL	Posterior cruciate ligament
PM	Posteromedial
POL	Posterior oblique ligament
PMC	Posterior medial Capsule
PLC	Posterior lateral Capsule
OPL	Oblique popliteal ligament
LCL	Lateral collateral ligament
ALL	Anterolateral ligament
FFL	Fabellofibular ligament
sMCL	Superficial medial collateral ligament
sMCL_Prox_A	Anterior proximal fiber of superficial medial collateral ligament
sMCL_Prox_C	Center proximal fiber of superficial medial collateral ligament
sMCL_Prox_P	Posterior proximal fiber of superficial medial collateral ligament
sMCL_Dist_A	Anterior distal fiber of superficial medial collateral ligament
sMCL_Dist_C	Center distal fiber of superficial medial collateral ligament
sMCL_Dist_P	Posterior distal fiber of superficial medial collateral ligament
POL_A	Anterior fiber of posterior Oblique Ligament
POL_C	Center fiber of posterior Oblique Ligament
POL_P	Posterior fiber of posterior Oblique Ligament
ACL_1 to ACL_6	Fiber number of anterior cruciate ligament
PCL_1 to PCL_7	Fiber number of posterior cruciate ligament
OPL_PL	Posterolateral fiber of oblique popliteal ligament
OPL_DL	Distal lateral fiber of oblique popliteal ligament

PMC_M	Medial fiber of posterior medial capsule
PMC_C	Central fiber of posterior medial capsule
PMC_L	Lateral fiber of posterior medial capsule
PLC_M	Medial fiber of posterior lateral capsule
PLC_C	Central fiber of posterior lateral capsule
PLC_L	Lateral fiber of posterior lateral capsule
MM_MedMeniscPost	Medial posterior ligament of medial meniscus
MM_MedMeniscAnt	Medial anterior ligament of medial meniscus
MM_MedMeniscCent	Medial central ligament of medial meniscus
MM_AntMeniscLat	Anterior lateral ligament of medial meniscus
MM_AntMeniscMed	Anterior medial ligament of medial meniscus
MM_PostMeniscLat	Posterior lateral ligament of medial meniscus
MM_PostMeniscMed	Posterior medial ligament of medial meniscus
MM_PostHorn	Posterior horn ligament of medial meniscus
MM_AntHorn	Anterior horn ligament of medial meniscus
LM_PostHorn	Posterior horn ligament of lateral meniscus
LM_AntHorn	Anterior horn ligament of lateral meniscus
LM_LatCoron	Lateral coronary ligament of lateral meniscus

Summary of input data

The following data obtained from a single knee specimen (DU02) as part of the Natural Knee Data Project at the University of Denver will be used:
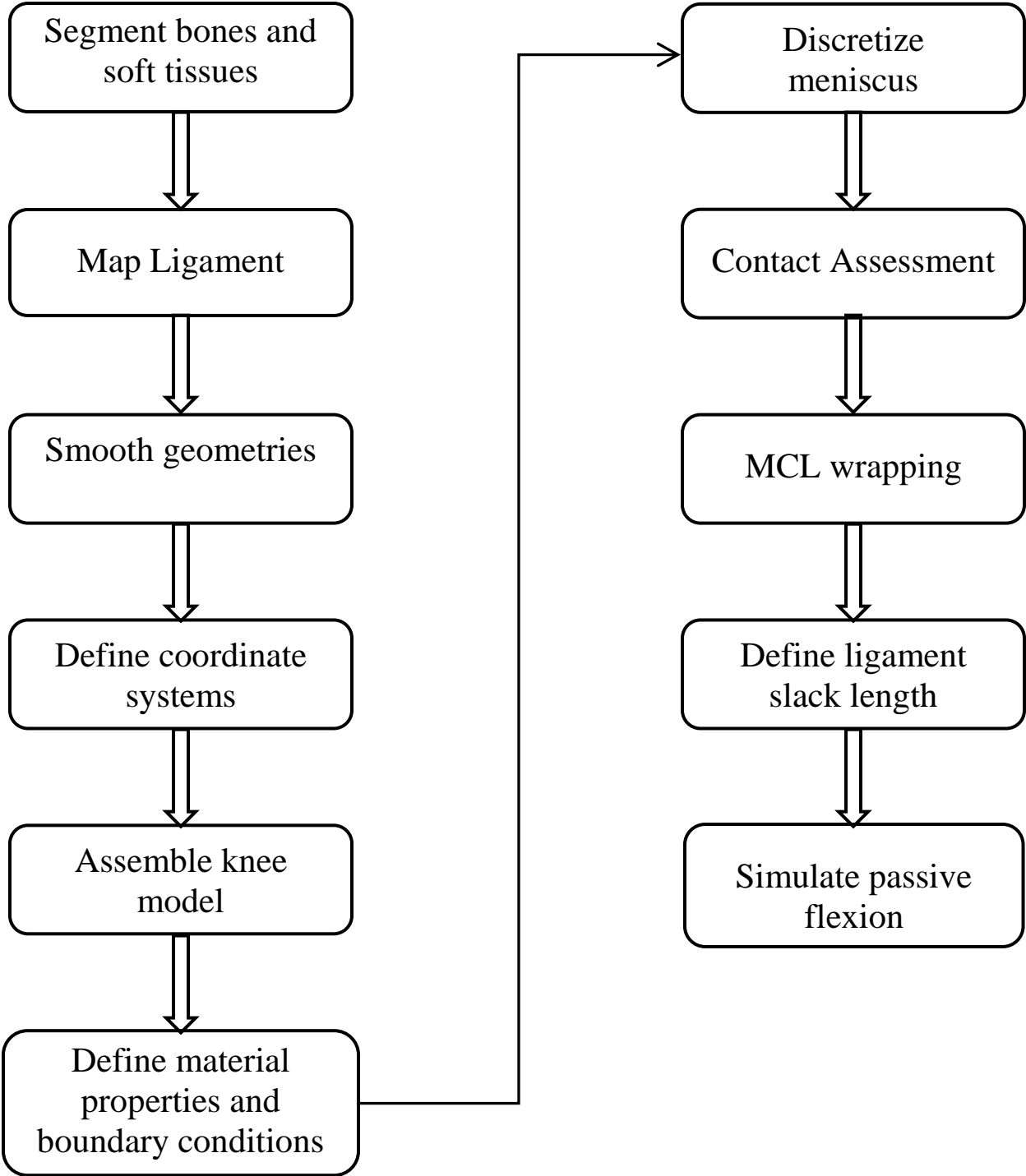
Knee Specimen Demographics:

- Right knee
- Age: 44 years
- Gender: Male
- Height: 1.83 m
- Weight: 70.31 kg
- BMI: 21.02

Specimen-specific medical imaging data sets:

- CT sequence of images in DICOM format_06mm
- MRI sagittal sequence of images in DICOM format

Overview of workflow for model development and outputs

Flow chart of the workflow for model development:

```
┌─────────────────────┐              ┌─────────────────────┐
│  Segment bones and  │─────────────▶│     Discretize      │
│     soft tissues    │              │      meniscus       │
└─────────────────────┘              └─────────────────────┘
          │                                     │
          ▼                                     ▼
┌─────────────────────┐              ┌─────────────────────┐
│    Map Ligament     │              │ Contact Assessment  │
└─────────────────────┘              └─────────────────────┘
          │                                     │
          ▼                                     ▼
┌─────────────────────┐              ┌─────────────────────┐
│  Smooth geometries  │              │    MCL wrapping     │
└─────────────────────┘              └─────────────────────┘
          │                                     │
          ▼                                     ▼
┌─────────────────────┐              ┌─────────────────────┐
│  Define coordinate  │              │  Define ligament    │
│      systems        │              │    slack length     │
└─────────────────────┘              └─────────────────────┘
          │                                     │
          ▼                                     ▼
┌─────────────────────┐              ┌─────────────────────┐
│   Assemble knee     │              │  Simulate passive   │
│       model         │              │      flexion        │
└─────────────────────┘              └─────────────────────┘
          │
          ▼
┌─────────────────────┐
│  Define material    │
│  properties and     │───────────────┐
│ boundary conditions │
└─────────────────────┘
```

Overview of Workflow for model development and outcomes

Knee Geometries and Ligament Insertions

The MRI and the CT images of the distal femur and proximal tibia were imported into image processing software (Mimics, Materialise, Inc., Belgium). The bone, cartilage, and meniscus geometries were manually masked, and 3D geometries were calculated. The surfaces were then smoothed using a filtering feature (remove spikes) available in Geomagic Studio (Geomagic, Inc., Research Triangle Park, NC), which detected and flattened single-point spikes on the surface mesh.

The insertions of the fibers used to represent each ligament were obtained from the MRI and CT images and from the literature (Giffin, Haemmerle et al. 2002; De Maeseneer, Van Roy et al. 2004; LaPrade, Engebretsen et al. 2007; LaPrade, Morgan et al. 2007; Lopes, Ferretti et al. 2008; Tajima, Nozaki et al. 2009; Ziegler, Pietrini et al. 2011; Claes, Vereecke et al. 2013). The ACL consisted of six fibers with the tibial insertions of the fibers divided into anteromedial (AM), anterolateral (AL), and posterolateral (PL) groups based on the description by Butler et al. (Butler, Guan et al. 1992). The femoral insertions of the fibers were placed halfway between the lateral intercondylar ridge (i.e., resident's ridge) and the posterior femoral cartilage (Hutchinson and Ash 2003; Sasaki, Ishibashi et al. 2012; Mochizuki, Fujishiro et al. 2014; Tsukada, Fujishiro et al. 2014). The three most proximal femoral insertions were connected to the AM and AL insertion groups on the tibia. The three most distal femoral insertions were connected to the PL group of tibial insertions. These connections were based on the fiber-level dissection of the ACL by Hara et al. (Hara, Mochizuki et al. 2009).

The PCL was represented with seven fibers. The tibial insertions of the PCL fibers were divided into anterolateral (AL) and posteromedial (PM) groups (Tajima, Nozaki et al. 2009). The

femoral insertions were located along the medial intercondylar ridge (Lopes, Ferretti et al. 2008). The four insertions closest to the posterior cartilage on the lateral aspect of the medial femoral condyle were connected to the PM group of tibial insertions. The three insertions closest to the femoral intercondylar ridge were connected to the AL group of tibial insertions.

The sMCL was divided into distal and proximal groups; each group was modeled with three fibers. The Posterior oblique ligament (POL), medial posterior capsule (MPC), and lateral posterior capsule (LPC) were each described by three fibers spanning the area that they cover (LaPrade, Morgan et al. 2007). The oblique popliteal ligament (OPL) was divided into posterior and distal fibers (LaPrade, Morgan et al. 2007). The lateral collateral ligament (LCL), the anterolateral ligament (ALL), and the fabellofibular ligament (FFL) were each represented with one fiber (LaPrade, Morgan et al. 2007; Claes, Vereecke et al. 2013). The horn attachments of the medial and lateral menisci were also modeled with one fiber each. Seven fibers represented the attachments of the coronary ligaments from the medial meniscus to the tibial plateau. The lateral coronary attachment was represented by one fiber.

All knee geometries and ligament insertions were transformed to the femoral coordinate system. This process enabled the use of a common anatomical coordinate system to compare the kinematics measured in the physical experiment to those predicted by the computational model.

Multibody Knee Model

The geometries of the bones, articular cartilage, menisci, and ligament insertions represented in the femoral coordinate system were imported into a multibody dynamics software called Automated Dynamic Analysis of Mechanical Systems (ADAMS 2013, MSC Software, Newport Beach, CA). Bone mass was based on the mean reported bone density of 1600 kg/m^3

(Galante, Rostoker et al. 1970) and was assumed to be uniformly distributed throughout each bone geometry. Cartilage-cartilage contact and menisci-cartilage contact were modeled using the ADAMS default IMPACT function. This algorithm generates contact force as a non-linear function of penetration depth and penetration velocity at the locations where contact was detected between rigid bodies. The contact parameters were defined previously (Imhauser, Siegler et al. 2008; Guess, Thiagarajan et al. 2010; Kia, Stylianou et al. 2014).

To define structural properties of the menisci, the lateral and medial meniscal geometries were first discretized circumferentially resulting in 34 and 31 elements, respectively, following the method of Guess et al. (Guess, Thiagarajan et al. 2010). A linear stiffness matrix was then used to connect neighboring elements, yielding multibody representations of deformable meniscal geometries (Guess, Thiagarajan et al. 2010).

Ligament fibers were represented by straight-line force elements connecting their tibial and femoral insertions. The structural properties of each ligament fiber were described using a tension-only, non-linear force-elongation relationship (Eqs. 1a, b),

$$F(l, \dot{l}, l_0) = \frac{1}{n}\{[f^*(l) + c_d \dot{l} B_1]B_2 + [K(l - (l_0 + \Delta_t)) + f^*(l_0 + \Delta_t) + c_d \dot{l} B_1]B_3\} \qquad (1a)$$

$$
\begin{aligned}
B_1 &= step(\dot{l}, 0, 0, \dot{l} + 0.1, 1) \\
B_2 &= step(l, l_0, 0, l_0 + 0.1, 1) \times step(l, (l_0 + \Delta_t), 1, (l_0 + \Delta_t) + 0.001, 0) \\
B_3 &= step(l, (l_0 + \Delta_t), 0, (l_0 + \Delta_t) + 0.001, 1)
\end{aligned}
\qquad (1b)
$$

where n is based on the number of fibers and their arrangement (Blankevoort and Huiskes 1996), l is the inter-insertional distance, $\dot{l}$ is the first derivative of the inter-insertional distance with respect to time, and l_0 is the ligament slack length. $f^*(l)$ is a cubic spline representing the ligament force-displacement response in the toe region. It was obtained by directly digitizing plots of the ligament force-displacement response from the literature (Butler, Guan et al. 1992; Harner,

Xerogeanes et al. 1995; Robinson, Bull et al. 2005; Wilson, Deakin et al. 2012) (GraphClick, Arizona Software, AZ). K represents the linear portion of the force-displacement response (Butler, Guan et al. 1992; Harner, Xerogeanes et al. 1995; Robinson, Bull et al. 2005; Hauch, Villegas et al. 2010; Wilson, Deakin et al. 2012). The transition between the toe region and linear region is defined by Δ_t. Each force element also included a parallel damping term (c_d = 1.5 Ns/mm) based on the stress relaxation response of ligaments (Funk, Hall et al. 2000). The step functions B_1, B_2, and B_3 are cubic polynomials that allow continuous and smooth generation of tensile forces as a ligament fiber becomes taut. The location dependent structural properties of the AM, AL, and PL groups of the ACL were defined based on the work of Butler et al (Butler, Guan et al. 1992). The structural properties of the ALL were assumed to be half of the LCL based on the observation that the ALL is thinner and less stout than the LCL and structural testing from the literature(Kennedy, Claes et al. 2015). The structural properties of the posterior capsule were described using a cubic spline fit to the properties of the sMCL (Robinson, Bull et al. 2005), since both have a stout appearance based on visual inspection. The horn attachments of the menisci were modeled with a linear tension-only force-elongation response and a stiffness of 180 N/mm (Hauch, Villegas et al. 2010). Tibiomeniscal coronary ligaments were also modeled as tension-only linear springs on the medial and lateral side with a stiffness about half that of the sMCL. The transverse intermeniscal ligament was not modeled due to its non-stout appearance during dissection of previous cadaver knees.

A generalized reduced gradient optimization algorithm was utilized to determine the slack lengths (l_0) of the ligament fibers (Lasdon, Fox et al. 1974). This optimization included the 29 fibers comprising nine ligaments that were observed to be taut at full extension or that carried force at full extension in our previous cadaveric experiments. The goal of the optimization was to

identify l_0 as a percentage of the fiber length at full extension (l_e) in the groups of fibers comprising each ligament. The objective function described the differences between the resultant ligament forces predicted by the model (F_i^m) and the experimentally-measured ligament forces at full extension (F_i^e) (Eq. 2a). The predicted ligament force was the resultant vectoral magnitude of force in the fibers that comprised each ligament. Altogether, l_0 was optimized for 29 fibers across nine ligaments in this underdetermined system of equations (Eq. 2a). The initial value of l_0 was defined to be the fiber length at full extension, and l_0 was allowed to vary by $\pm 10\%$ from the initial value (Eq. 2b).

$$\min \sum_{i=1}^{9} \left(\left[\sum_{j=1}^{a} [\vec{F}_{i,j}^m(l,\dot{l},l_0)]^2 \right]^{\frac{1}{2}} - F_i^e \right)^4 \tag{2a}$$

$a =$ number of fibers comprising each of the 9 ligaments included in the optimization

$F_i^m = \{ACL, sMCL, LCL, FFL, OPL, POL, MPC, LPC, PCL_{PM}\}$
$F_i^e = \{37, 4, 20, 1, 10, 18, 1, 4, 10\}\ N$
$a = \{6, 6, 1, 1, 2, 3, 3, 3, 4\}\ fibers$

$$l_0 = l_e(100 - x)\% \qquad -10 \le x \le +10 \tag{2b}$$

The optimization was performed with the knee at full extension while permitting the tibia to move in the proximal-distal direction under 10 N of compression. This resolved any penetration between the cartilage and meniscal surfaces as well as the opposing cartilage surfaces. The remaining degrees of freedom were held constant matching those of the predefined position and orientation of the knee at full extension.

The groups of proximal and distal fibers comprising the sMCL were each assigned to carry the experimentally measured force in the entire sMCL since they were in series. The posteromedial fibers of the PCL were included in the optimization to achieve a target force at full extension that

was measured in our previous work (Kia, Schafer et al. 2016) because force at full extension because these fibers were observed during dissection of the knee to be taut at full extension.

Ligaments that were observed to be slack during previous in vitro dissection studies by our group or that did not carry force at full extension in our previous cadaveric experiments were not included in the optimization. The anterolateral fibers of the PCL were observed to be slack at full extension in our previous studies; therefore, their slack lengths were increased by 10% of their length at full extension. The ALL was also observed to be slack at full extension in our previous cadaveric dissections; therefore, the slack length of the ALL fiber was increased by 15% of its length at full extension. The slack lengths of all fibers of the coronary ligaments were assumed to be their lengths at full extension. The fibers of the medial and lateral posterior capsule were slack with flexion in the experiment; thus, these groups were deactivated at flexion angles $> 30°$.

Wrapping of the sMCL was modeled by connecting its proximal and distal fiber groups with 1 mm diameter spheres located ~10 mm below the joint line. Each sphere was constrained tangent to the proximal surface of the tibia via a planar joint and within this plane using a linear spring. These springs were assigned a stiffness ten times less than that of the sMCL based on the weak connection that we observed between the sMCL and the proximal tibia when during previous cadaveric dissections. The anterior and posterior spheres were constrained to the central sphere with a transverse spring. These springs simulated the transvers properties of the sMCL as characterized by Weiss et al. (Quapp and Weiss 1998)

Simulation of Passive Knee Flexion

Fix the femur in all directions except for rotation about its transepicondylar axis. Fix the tibia in flexion, but leave it free to translate and rotate in all other directions. Model passive flexion by rotating the femur about its transepicondylar axis from full extension to 130° of flexion at a rate of 1.35°/sec while applying 10 N of compression. Rotate the femur at this angular velocity to model the slow loading rate used in previous robotic experiments.

Solver Parameters

The equations of motion were generated and solved using ADAMS. Selecting runtime and solver parameters (GSTIFF integrator)(Gear 1971) including an integrator error of 0.001, the maximum number of iterations of ten, and initial simulation step size of 0.005 s. The simulation required 85 minutes to complete using a desktop PC (3 GHz Intel Xeon E5-1607 Processor) with 24 GB of RAM.

Modeling and Simulation (M&S) outputs

Measured resultant force borne by knee ligaments (ACL, PCL , LCL, sMCL, and POL) were measured. The kinematics outcomes were: 1) transverse plane motion including internal-external rotation; 2) sagittal plane motions including posterior-anterior and proximal-distal translations, and 3) frontal plane motions including medial-lateral translation and varus-valgus rotation; all of which were described using a convention that we adapted from Grood and Suntay (Grood and Suntay 1983). The model outputs were discretized into 1° increments.

Software and hardware requirements

Specific software and hardware used to implement our protocol are summarized below.

1- **Software requirements**

    a- Mimics Research 20.0; Materialise, Leuven, Belgium (older versions can work as well)

    b- Geomagic Studio 2013, Morrisville, NC, USA

    c- ADAMS 2013, MSC software, CA, USA

    d- Matlab R2013b, MathWorks, Natrick, Massachusetts, USA

2- **Hardware requirements:**

Desktop PC (3 GHz Intel Xeon E5-1607 Processor) with ≥ 24 GB of RAM or higher

3- **Anticipated man hours and expertise level**

It is recommended to start using this protocol after finishing tutorial kits provided by ADAMS and Mimics (MSCsoftware 2012; Materialise 2013). Also, the user is recommended to have moderate experience in using Matlab and basic knowledge of the knee anatomy and multibody dynamics analysis. The anticipated time for developing a knee model is as follows:

    a- For an expert in ADAMS, Mimics, Geomagic, and knee anatomy, the time required is approximately two weeks.

    b- For a beginner in ADAMS, Mimics, Geomagic, and knee anatomy, the time required is approximately 8 to 10 weeks.

4- **Computational cost**

If you are running ADAMS 13 on a PC with the aforementioned specifications, it will take 60 to 80 minutes to complete a simulation of passive flexion.

Segmentation of bone, cartilage, and meniscus

We used MIMICS for processing MRI data, which includes segmentation of the following tissues:

1- Bones: femur, tibia, and patella
2- Cartilages: femur, tibia, and patellar cartilage
3- Meniscus: medial and lateral

Bone segmentation:

Segment the bone geometries from the sagittal MRI sequence and use them to build the model. Also segment the bone geometries from CT to check the quality of the bony geometries obtained from MR; specifically, compare the volume of the bony geometries obtained from MRI and CT as well as their surfaces using Geomagic. First, create separate masks for the femur, tibia, and patella. Next, manually use the 'livewire' tool to edit the masks by cycling between both the axial and sagittal views. Cycle through each slice and use your best judgment to identify the voxels that belong to the bone based on the voxel color. Fill in the slice at the most distal tibia and the most proximal femur in the axial view. Then, use the function: 'Calculate 3D' to calculate all 3D cartilage geometries using the Quality setting: 'Optimal' (Fig. 1). Visually inspect the geometry of the femur, the tibia, and the patella for any holes or gaps. Then, use the 'Wrap' function to obtain closed cartilage geometries using the following settings: 'Smallest Detail: 0.5 mm' and 'Gap Closing Distance: 3.0 mm' (Fig. 2). Finally, export the three geometries as ASCII STL files.
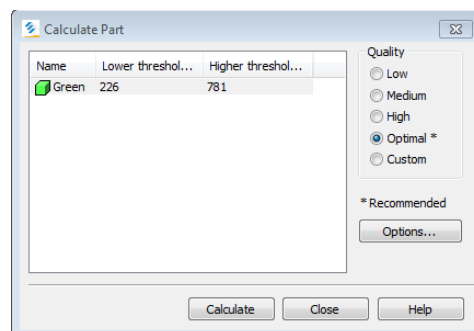
Fig. 1: Settings for 3D calculation of the geometries in Mimics
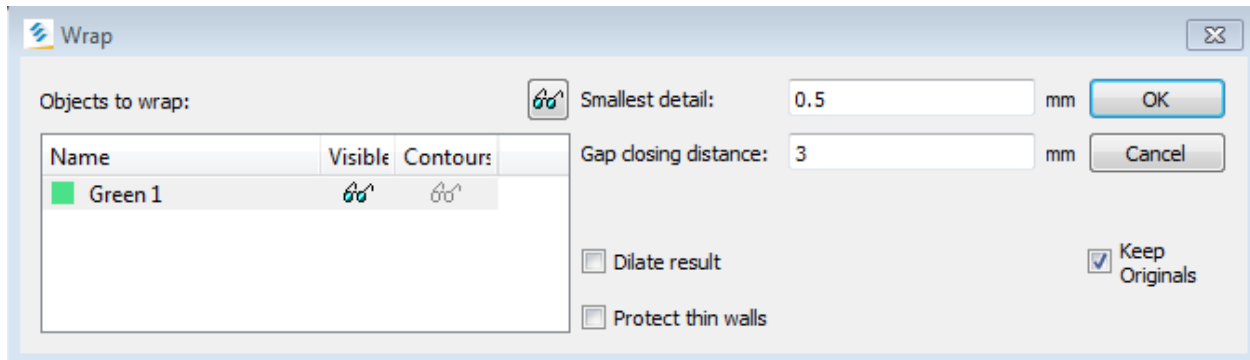
Fig. 2: Settings of the 'Wrap' function in Mimics

Cartilage segmentation:

In cartilage segmentation, use the soft tissue imaging-sagittal plane MRI sequence and create separate masks for the femoral, tibial, and patellar cartilages. Next, use the 'livewire' tool to manually edit the masks by cycling between both the coronal and sagittal views. Go slice by slice and use your best judgment to identify the voxels that belong to the cartilage (gray voxels) (Fig. 3 and 4). Then, use the function: 'Calculate 3D' to calculate all 3D cartilage geometries using the 'Quality' setting: 'Optimal' (Fig. 1). Inspect the geometries of the femoral, tibial, and patellar cartilages for any holes or gaps. Finally, use the 'Wrap' function to obtain closed cartilage geometries with the following settings: 'Smallest Detail, 0.5 mm' and 'Gap Closing Distance: 3.0 mm' (Fig. 2). Then, export the geometries as ASCII STL files.

Subsequently, split the femoral cartilage into medial and lateral portions to separately measure the contact forces on the medial and lateral condyles and to decrease simulation time by reducing the number of combinations that the contact algorithm must search through.
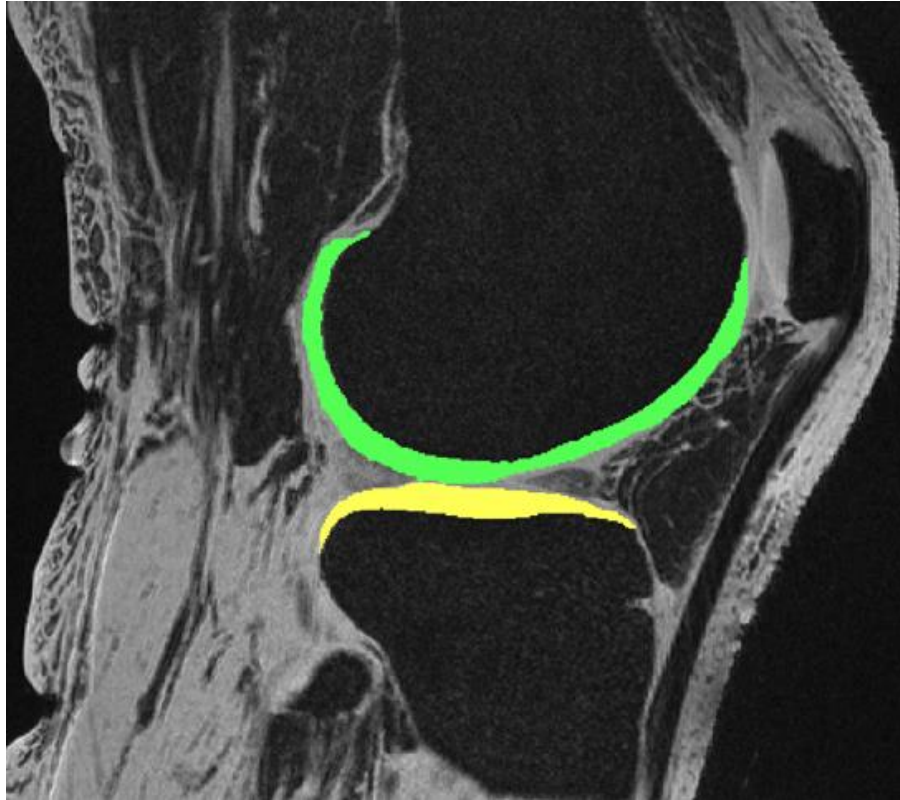
Fig. 3: Masking the femoral and tibial cartilage in Mimics
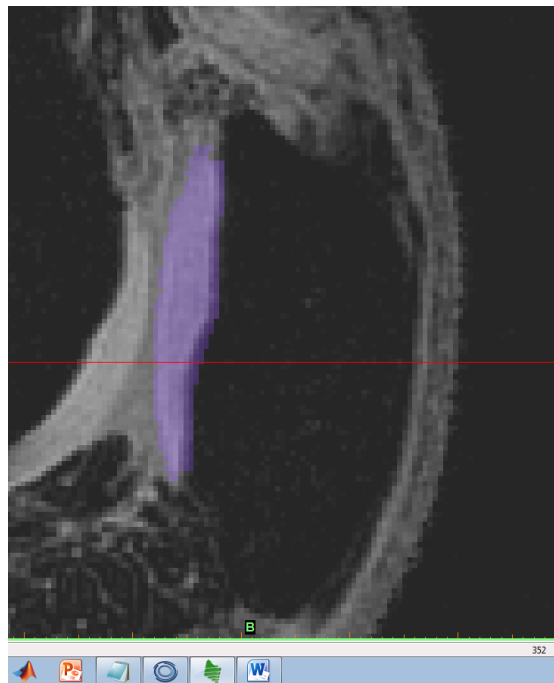
Fig. 4: Masking the patellar cartilage in Mimics

Meniscus segmentation:

Use the soft tissue imaging-sagittal plane MRI sequence to segment the medial and lateral menisci using independent masks. Use the 'Livewire' tool to edit the masks by cycling between both the coronal and sagittal views. Go slice by slice and use your best judgment to identify the voxels that belong to each meniscus (darker gray) (Fig. 5). Then, calculate the 3D parts of the menisci by selecting 'Optimal' quality for both masks. Finally, use the 'Wrap' function to obtain closed cartilage geometries using the following settings: 'Smallest Detail: 0.5 mm' and 'Gap Closing Distance: 3.0 mm' (Fig. 2). Export the two geometries as ASCII STL files.

Fig. 5: Masking the meniscus in Mimics

Mapping ligament insertions

Define the origins and the insertions of the fibers used to represent each meniscal attachment and ligament using landmarks from the MR and CT images. The landmarks used to identify the insertions of the ligaments were based on data in the literature as summarized on our previous work (Kia, Schafer et al. 2016). Specifically, model the horn attachments of the medial and lateral menisci with one fiber each (Fig. 6a). Represent the attachments of the coronary ligaments from the medial meniscus to the tibial plateau using seven fibers (two anterior, three medial, and two posterior) to constraint the medial meniscus to the tibial plateau (Fig. 6a). Represent the lateral coronary ligament by one fiber to constraint the lateral meniscus to the tibia/fibula (Fig. 6b). The ACL consisted of six fibers with the tibial insertions of the fibers divided into anteromedial (AM), anterolateral (AL), and posterolateral (PL) groups based on the description by Butler et al. (Butler, Guan et al. 1992) (Fig. 7a). Place the femoral insertions of the fibers halfway between the lateral intercondylar ridge (i.e., resident's ridge) and the posterior femoral cartilage (Sasaki, Ishibashi et al. 2012; Mochizuki, Fujishiro et al. 2014). Connect the three most proximal femoral insertions to the AM and AL insertion groups on the tibia. Connect the three most distal femoral insertions to the PL group of tibial insertions. These connections were based on the fiber-level dissection of the ACL by Hara et al. (Hara, Mochizuki et al. 2009) and dissections performed in our laboratory. Represent the PCL with seven fibers and divide their tibial insertions into anterolateral (AL) and posteromedial (PM) groups (Tajima, Nozaki et al. 2009) (Fig. 7b). Place the femoral insertions along the medial intercondylar ridge (Lopes Jr, Ferretti et al. 2008). Connect the four insertions closest to the posterior cartilage on the lateral aspect of the medial femoral condyle to the PM group of tibial insertions. Connect the three insertions closest to the femoral intercondylar ridge to the AL group of tibial insertions. Divide the sMCL into distal and proximal groups; model each group with three fibers (Fig. 7c). Describe the POL, MPC, and LPC by three fibers each that spanning the area that they cover (LaPrade, Morgan et al. 2007) (Fig.s 7c, and 7d). Divide the oblique popliteal ligament (OPL) into posterior and distal fibers (Fig. 7e). Represent the LCL, ALL, and FFL with one fiber each (LaPrade, Ly et al. 2003; LaPrade, Morgan et al. 2007; Claes, Vereecke et al. 2013) (Fig. 7f).
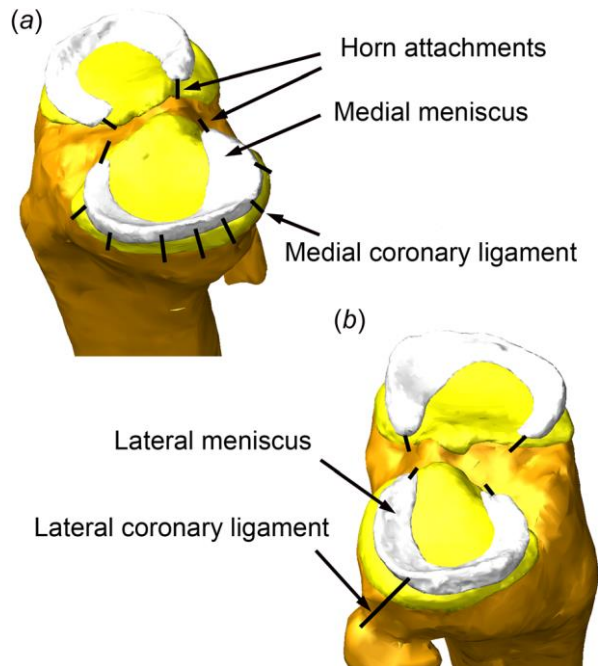
Fig. 6: (a) The anterior and posterior horn attachments of the menisci were each represented by one fiber (total of four fibers). The coronary ligaments were represented by seven fibers (two anterior, three medial, and two posterior) constraining the medial meniscus to the tibial plateau. (b) One fiber represented the coronary ligament constraining the lateral meniscus to the tibia/fibula.
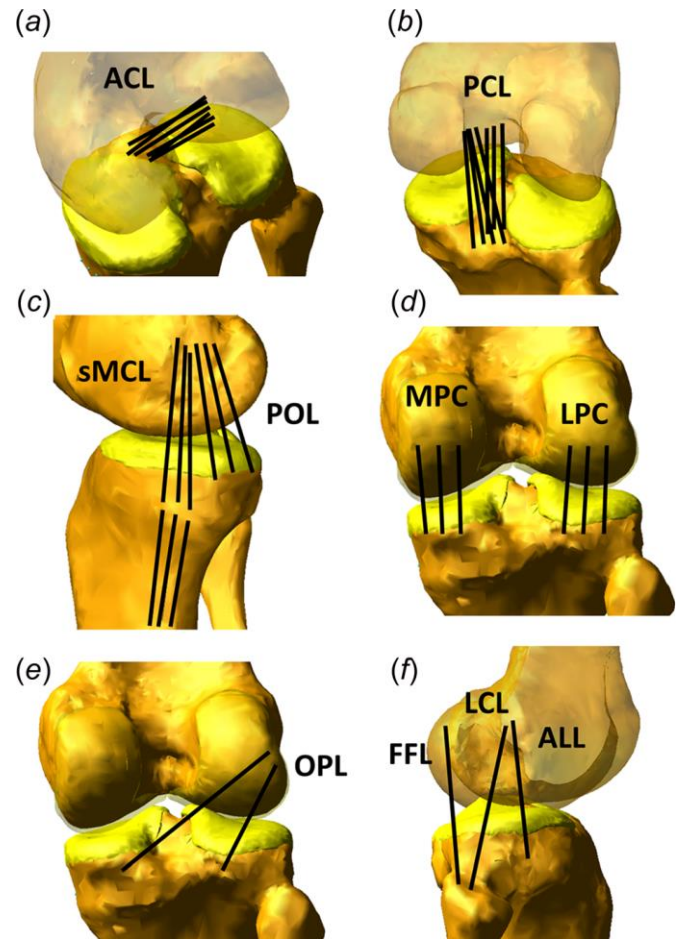

Fig. 7: Fibers representing the ligaments in the multibody model: (a) ACL (six fibers), (b) PCL (seven fibers), (c) sMCL (three proximal fibers and three distal fibers), POL (three fibers), (d) MPC and LPC (three fibers each), (e) OPL (two fibers), (f)FFL (one fiber), LCL (one fiber), and ALL (one fiber)

The following name index will be used for each ligament fiber (see list of acronyms for their definitions):

Medial structures:

- sMCL_Prox_A, sMCL_Prox_C, sMCL_Prox_P
- sMCL_Dist_A, sMCL_Dist_C, sMCL_Dist_P
- POL_A, POL_C, POL_P

Lateral structures:

- LCL
- FFL
- ALL

Cruciate structures:

- ACL_1, ACL_2, ACL_3,ACL_4, ACL_5, ACL_6
- PCL_1, PCL_2, PCL_3,PCL_4, PCL_5, PCL_6, PCL_7

Posterior capsule structures:

- OPL_PL, OPL_DL
- PMC_M, PMC_C, PMC_L
- PLC_M, PLC_C, PLC_L

Medial Meniscal structures:

- MM_MedMeniscPost
- MM_MedMeniscAnt
- MM_MedMeniscCent
- MM_AntMeniscLat
- MM_AntMeniscMed
- MM_PostMeniscLat
- MM_PostMeniscMed
- MM_PostHorn
- MM_AntHorn

Lateral Meniscal structures:

- LM_PostHorn
- LM_AntHorn
- LM_LatCoron

Identifying the Femoral Insertions of the sMCL and the POL

- sMCL: Identify the depression (i.e., medial sulcus) just proximal and posterior to the medial epicondyle, where the insertion area is approximately 10 mm in diameter (Fig.s 8 and 9). Set the locations of the proximal MCL fibers to span this insertion area. Specifically, place the central MCL fiber at the deepest point of the medial sulcus. Place the insertions of the anterior and posterior fibers midway between the center fiber and the anterior and posterior borders of the medial sulcus, respectively (Fig. 8). Use two fibers each for the anterior, center, and posterior portions of the sMCL: one of these two fibers connects the distal insertion of the femur to the proximal insertion of the tibia and the other connects to the proximal insertion of the tibia to the distal insertion of the tibia.

- POL: On the medial aspect of the femur, identify the prominences of the gastrocnemius tubercle (GT) and the adductor tubercle (AT) (Fig. 9). The insertion area of the POL is just posterior and distal to the GT. Again, use an anterior, central, and posterior fiber to capture the width of the ligament insertion (Fig. 8). As described by LaPrade et al. (LaPrade, Ly et al. 2007), the center fiber of the POL originates on the femur roughly 7.7 mm distal and 6.4 mm posterior to the AT, and 1.4 mm distal and 2.9 mm anterior to GT. The area of insertion of the POL is on average 90 mm^2, and the anterior and posterior fibers are placed at the borders of this area (Fig. 8).
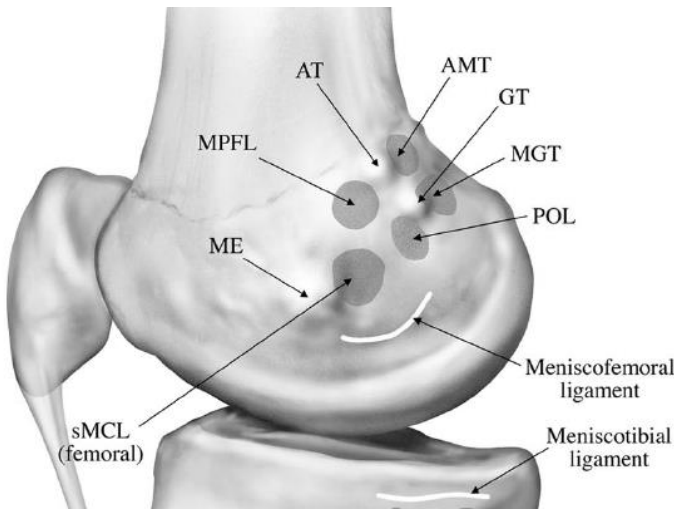
Fig. 9: the femoral osseous landmarks and attachment sites of the main medial knee structures. AT = adductor tubercle, GT = gastrocnemius tubercle, ME = medial epicondyle, AMT = adductor magnus tendon, MGT = medial gastrocnemius tendon, sMCL = superficial medial collateral ligament, MPFL = medial patellofemoral ligament, and POL = posterior oblique ligament (LaPrade, Ly et al. 2007)
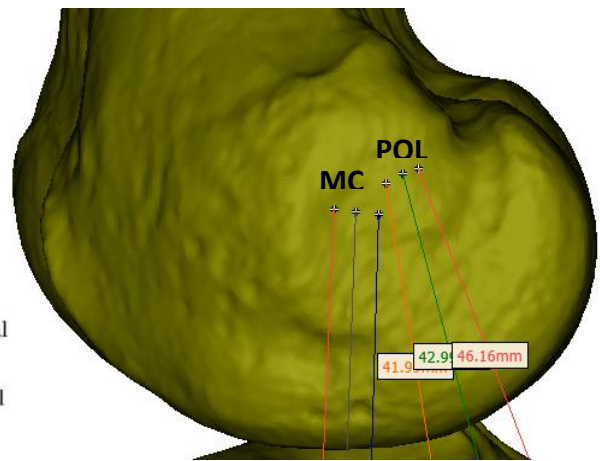
Fig. 8: Illustration of the proximal insertions of the medial collateral ligament (MCL) and the posterior oblique ligament (POL) in our model

Identifying the tibial insertions of the sMCL and POL

- **Distal tibial insertions of the sMCL:** Place the anterior fiber just anterior to the posteromedial crest about 60 mm distal to the joint line (Fig. 10). Place the center and posterior fibers' insertions about 3 and about 6 mm posterior to the anterior fiber, respectively to span the area described by Liu et al. for the distal insertion of the sMCL (Liu, Yue et al. 2010) (Fig. 11).

- **Proximal tibial insertions of the sMCL:** Approximate the line of action of the sMCL by attaching the distal fibers in the large depression about 10 mm distal to the tibial plateau (Fig. 11). Place the fibers anterior to posterior so that anterior fiber is adjacent to the anterior border of the distal sMCL (Fig. 10). On average. Place each of the three fibers about 7 mm apart in the AP direction to span the width of the sMCL.

- **POL (central arm):** Model the central arm of the POL as described by LaPrade et al. (LaPrade, Ly et al. 2007). Attach the 3 tibial fibers so they span the posteromedial corner of the tibia at the edge of the tibial plateau (Fig. 10). Place the anterior fiber of the POL adjacent to the posterior fiber of the proximal sMCL. Place the center and posterior fibers about 8 and 16 mm posterior, respectively, to the anterior fiber and located at the curvature of the tibial plateau, respectively.
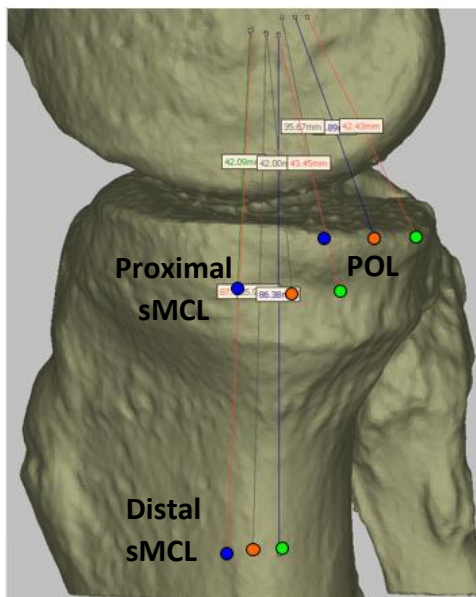
Fig. 11: Illustration of the tibial insertions of the proximal and distal superficial medial collateral ligament (sMCL), and the posterior oblique ligament (POL) in our model. Blue, orange, and green dots represent the location of insertions of the anterior, central, and posterior fibers, respectively.
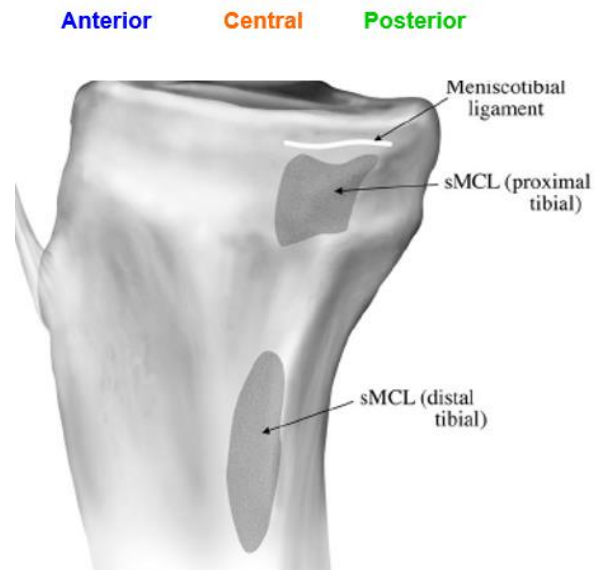
Fig. 10: Tibial insertions of the proximal and distal aspect of the superficial medial collateral ligament as illustrated by LaPrade (LaPrade, Ly et al. 2007). Anterior (in blue), central (in red), and posterior (in green) refer to the orientation of the tibia

Identifying the femoral insertions of the ACL:

Place the femoral insertion of all ACL fibers about halfway between the lateral intercondylar ridge (i.e., resident's ridge) and the posterior margin of the cartilage, which is located at the

posteromedial aspect of the lateral femoral condyle (Fig. 12). First, place the femoral insertion of fiber 1 at the top of the AM depression (Fig. 13). Next, place the femoral insertion of fiber 4 just distal to the bifurcate ridge, which may not be visible in all knees, but approximately bisects the length of the femoral insertion of the ACL from proximal to distal. Equally space fibers 5 and 6 to span the rest of the PL region from proximal to distal, placing fiber 6 just above the distal margin of the PL "fossa" (Fig. 13). Place fiber 2 a few mm distal to fiber 1. Equally space the insertions of fibers 2 and 3 between fibers 1 and 4 (Fig. 13).
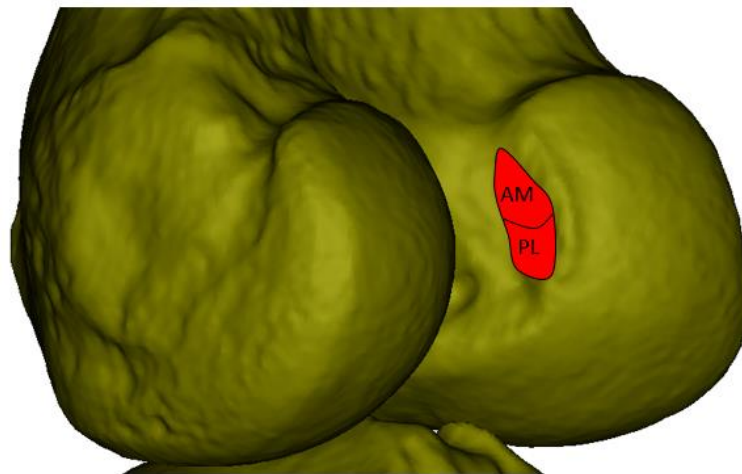
Fig. 12: Region of the femoral insertion of the anteromedial (AM) and posterolateral (PL) fibers of the ACL
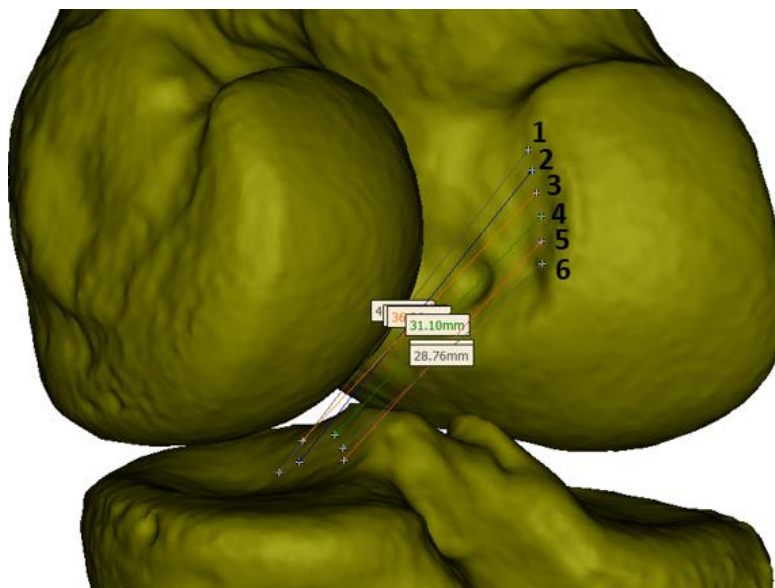
Fig. 13: Distribution of the femoral insertions of the six ACL fibers (ACL_1-6)

Identifying the tibial insertions of the ACL:

Using the ACL ridge as a guide, place the tibial insertions fibers 1 and 2 to span the medial-lateral dimension of the AM bundle depicted by Ziegler et al. (Ziegler, Pietrini et al. 2011) below (Fig. 14a). Follow the convention of Butler et al., who divided the ACL into three bundles (AL, AM, and PL) to characterize its structural properties regionally (Butler, Guan et al. 1992). Specifically, define fiber 2 to be the AL bundle, fibers 1 and 3 to comprise the AM bundle, and fibers 4, 5, 6 to comprise the PL bundle (Fig. 14b).

A=tubercle of anterior horn of medial meniscus
B=anterolateral fossa
C=attachment of anterior horn of lateral meniscus
D=ACL tubercle
E=ACL ridge
F=lateral tibial eminence
G=medial tibial eminence
H=retro-eminence ridge
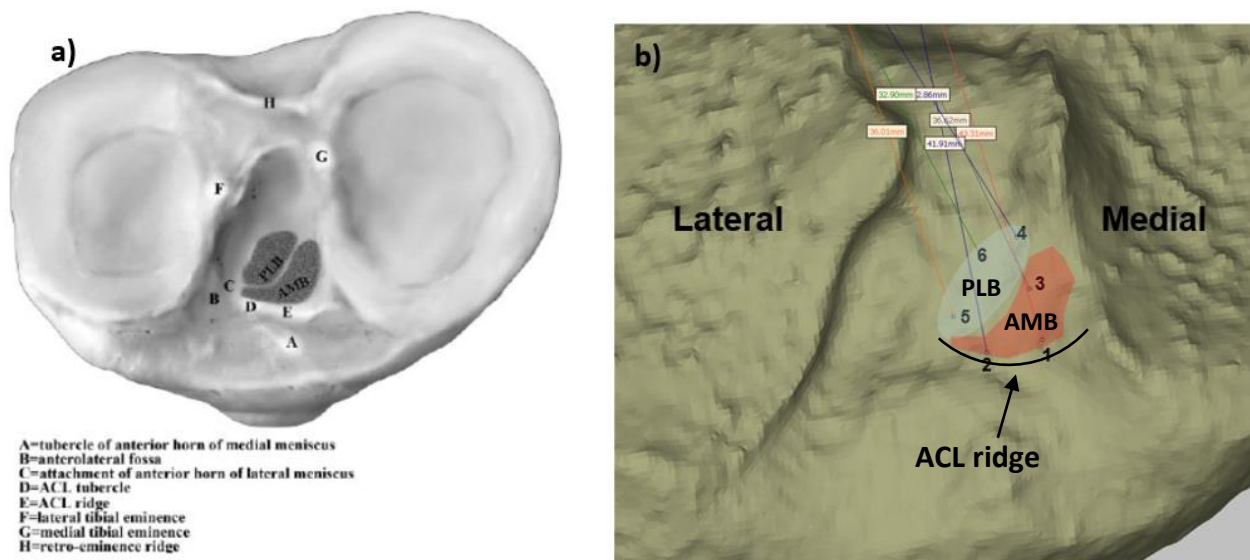
Fig. 14: a) Tibial insertion sites of the anteromedial bundle (AMB) and posterolateral bundle (ALB) as reported by Ziegler et al. (Ziegler, Pietrini et al. 2011); b) The tibial insertions of the six ACL fibers with respect to the AMB and PLB

Identifying the femoral insertion of the PCL:

Describe the PCL with 7 fibers; 4 fibers in the posteromedial (PM) site, and 3 fibers in the anterolateral (AL) site (Fig. 15). Evenly space the femoral insertions of these fibers across the AL and PM sites just distal to the medial intercondylar ridge. Differentiate the femoral insertion of the AL and PM fibers by the change in slope of the medial bifurcate ridge (Lopes Jr, Ferretti et al. 2008) (Fig. 15).
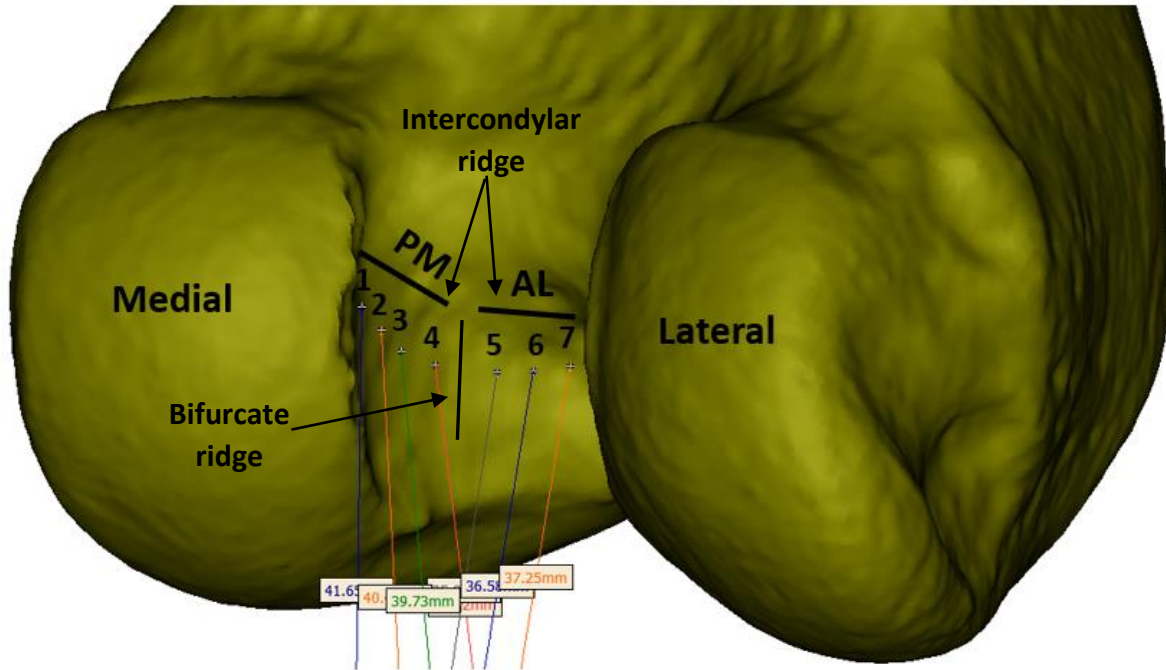
Fig. 15: Distribution of the seven PCL fibers at the femoral insertion, which was divided into posteromedial (PM) and anterolateral (AL) sites.

Identifying the tibial insertions of the PCL

The tibial insertions of the four PM fibers span the posterior margin of the posterior intercondylar fossa spanning about 12 mm in the medial-lateral (ML) direction (fibers 1-4, Fig. 16). The tibial insertions of the three AL fibers are about 5 mm anterior to the PM fibers and span about 7 mm in the ML direction (fibers 5-7, Fig. 16). Arrange them such that the tibial insertion of each AL fiber is slightly medial to the tibial insertion of PM fibers 2, 3, and 4 (Fig. 16).
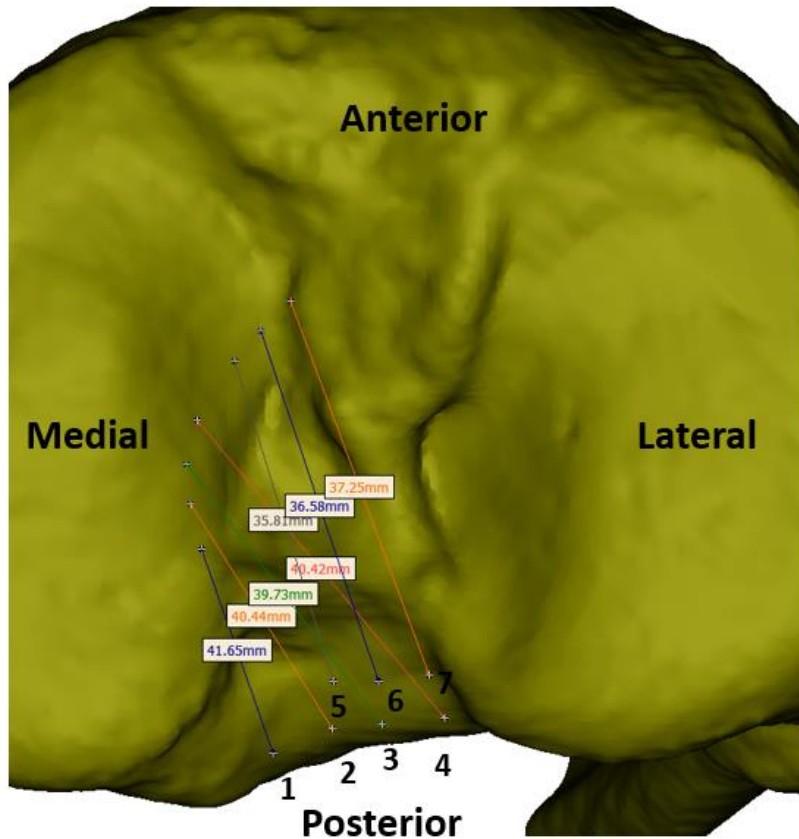
Fig. 16: Distribution of the tibial insertions of the seven PCL

Identifying the femoral and tibial insertions of the posterior capsule

To identify the femoral insertions of the posterior capsule, first look sagittally, and mark the most posterior point on the posterior aspect of the femoral condyle. Then, looking coronally and posteriorly, define the femoral insertion of posterior capsule to span the medial-lateral distance of the femoral cartilage (Fig. 17a and 17b). Locate the tibial insertions of the posterior capsule on the posterior, proximal edge of the tibial plateau. Place the tibial insertions of the posterior capsule to be directly distal to the femoral insertions so that the fibers of the posterior capsule are aligned vertically (Fig. 17a); the length of each vertical fiber is about 30 mm.
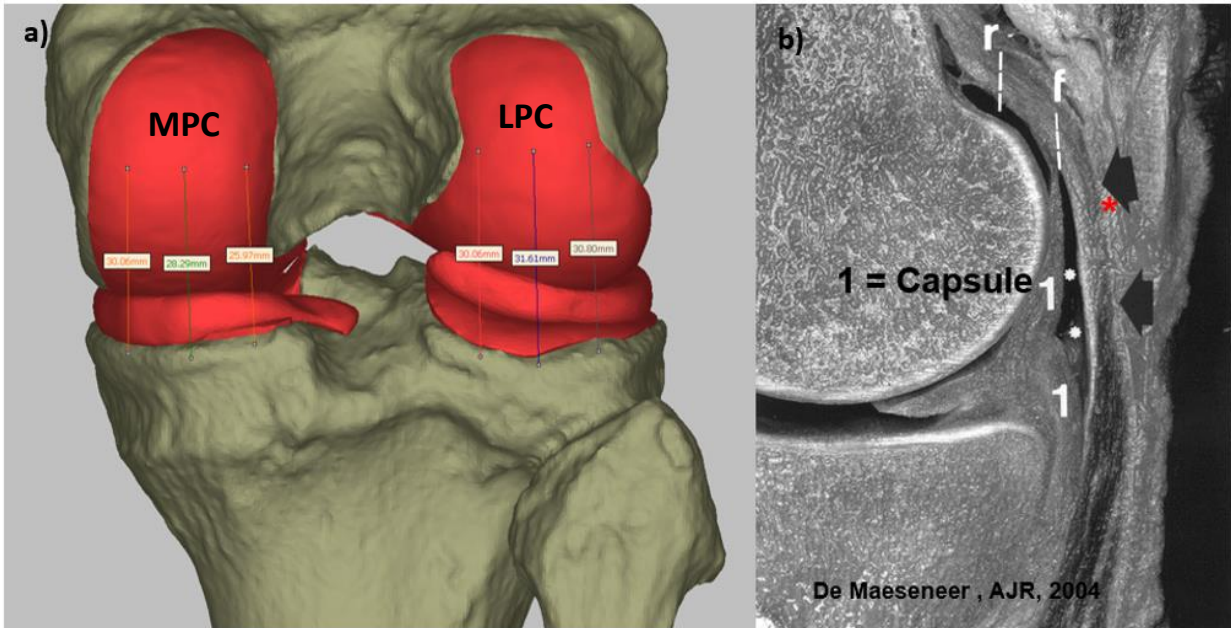
Fig. 17: (a) Proximal and distal insertions of the medial and lateral posterior capsule (MPC and LPC); (b) Insertions of the posterior capsule as reported by De Maeseneer et al. (De Maeseneer, Van Roy et al. 2004)

Identifying the insertions of the OPL:

- Define the posterolateral portion of the oblique popliteal ligament (OPL_PL) by connecting the femoral insertion of the PLC_C to the tibial insertion of the PMC_C (LaPrade, Morgan et al. 2007) (Fig. 18.a)

- The distal posterior portion of the oblique popliteal ligament (OPL_DL) was defined by connecting the femoral insertion of the PLC_C to the posterolateral corner of the posterior intercondylar fossa, which is about 13 mm medial to the tibial insertion of the PLC_M (Fig.18.a).
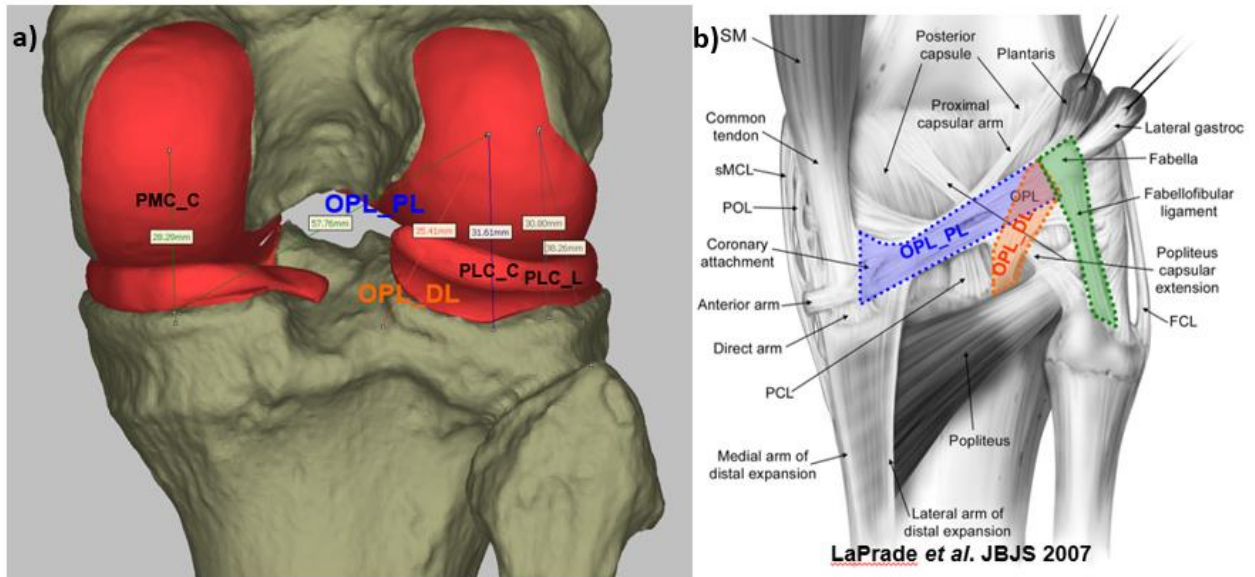
Fig. 18: a) femoral and tibial insertions of the proximal lateral (OPL_PL) and distal lateral (OPL-DL) oblique popliteal ligament; b) OPL_PL and OPL_DL as reported by LaPrade et al (LaPrade, Morgan et al. 2007)

Identifying the insertion of the lateral structures LCL, FFL, and ALL:

The LCL, FFL, and ALL are all represented by a single fiber.

- **LCL:** Locate the femoral insertion of the LCL at the minima of the sulcus (small bony depression) slightly proximal and posterior to the lateral epicondyle (Fig. 19). Place the distal insertion of the LCL at the minima of the sulcus on the lateral aspect of the fibular head (Fig. 19).

- **FFL:** Locate the femoral insertion of the FFL at the lateral edge of the lateral posterior condyle (Fig.s 18b and 19). Place the distal insertion of the FFL on the lateral aspect of the fibular head about 4 mm posterior to the fibular insertion of the LCL (Fig. 19).

- **ALL:** Locate the femoral insertion of the ALL just anterior to that of the LCL (Fig. 19). Place the tibial insertion of the ALL 5 mm distal to the tibial articular surface and about 22 mm posterior to Gerdy's tubercle (Vincent, Magnussen et al. 2012) (Fig. 19).

27
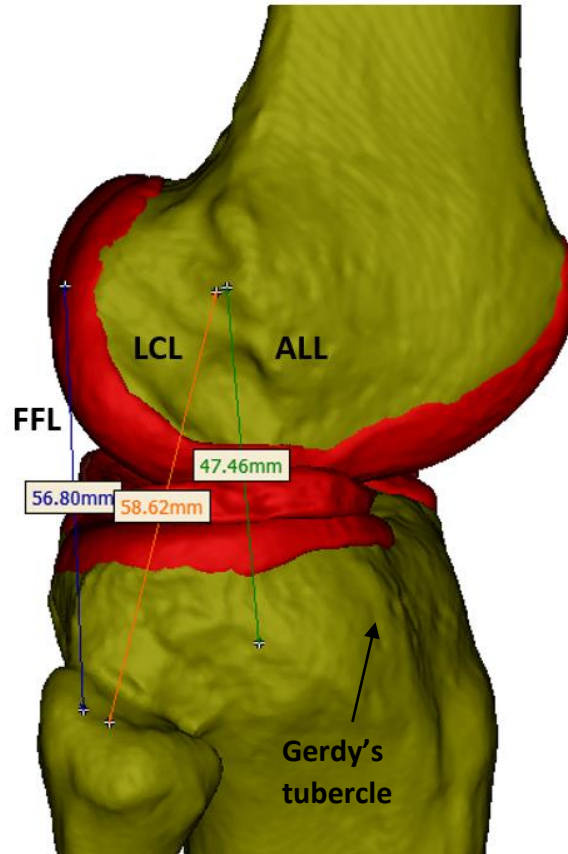
Fig. 19: The proximal and distal insertions of the lateral collateral ligament (LCL), fabellofibular ligament (FFL), and anterolateral ligament (ALL)

Identifying the lateral meniscal attachments:

Model the anterior and posterior horns of the lateral meniscus with a single fiber each (Fig. 20). These fibers permit the lateral meniscus to rotate, but resist lateral translation. Use one fiber each to connect the first and last radial section of the discretized geometry of the lateral meniscus to the tibial plateau. These two fibers are respectively located just anterior and posterior to the lateral tibial spine (Fig. 20).

Define one fiber (LatCoronaryLig) to represent the coronary ligament constraining the lateral meniscus to the tibia/fibula (Fig. 20). Thefibular insertion was located at the top of the fibular head, 5 mm posterior to the fibular insertion of the FFL. Its length is about 25 mm and it is inclined by an angle of about 25° with respect to the tibial long axis attaching to the most posterolateral aspect of the lateral meniscus (Fig. 6b).
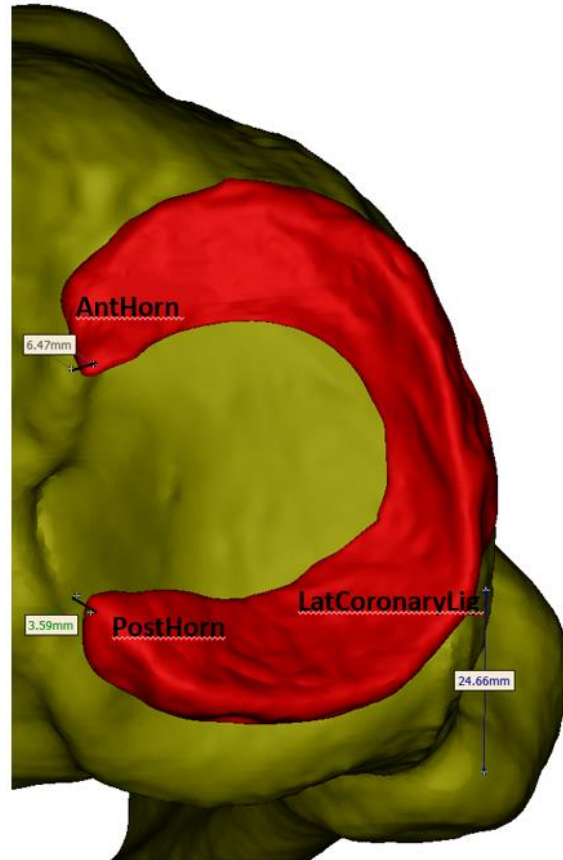
Fig. 20: The lateral meniscal attachments of the anterior horn, posterior horn, and the lateral coronary ligament

Identifying the medial meniscal attachments:

- Secure the medial meniscus to the tibial plateau using nine fibers. Two of these nine fibers define the anterior and posterior horns of the medial meniscus. Locate the posterior fiber just posterior to the medial tibial spine and locate the anterior fiber about 10 mm anterior to the medial tibial spine (Fig. 21).

- Use two posterior, two anterior, and three medial fibers to represent the coronary ligaments constraining the medial meniscus to the tibial plateau (Fig. 21). These seven fibers secure the meniscus to the tibia on all sides leaving it relatively immobile. These fibers simulate the capsular connections between the meniscus and the tibia. As for the two anterior fibers, position the meniscal insertion of the most anterior fiber (MM_AntMeniscLat) about 20 mm medial to the anterior horn of the medial meniscus (MM_AntHorn) on the outer aspect of the medial meniscus (Fig. 21). Position the meniscal insertion of the more medial and

anterior fiber (MM_AntMeniscMed) about 10 mm medial to the most anterior fiber (MM_AntMeniscLat) (Fig. 21). As for the three fibers on the medial aspect of the medial meniscus, Place the meniscal insertion of the MM_MedMeniscAnt 10 mm posterior to the MM_AntMeniscMed meniscal insertion. Place the meniscal insertion of the central fiber on the most medial aspect of the medial meniscus (MM_MedMeniscCent). Place the meniscal insertion of the most posterior of these three fibers (MM_MedMeniscPost) about 18 mm posterior to the MM_MedMeniscCent meniscal insertion. As for the two posterior fibers, place the meniscal insertion of the MM_PostMeniscMed 10 mm posterior and lateral to the most posterior of the medial fibers (MM_MedMeniscPost). The meniscal insertion of the most posterior and lateral fiber (MM_PostMeniscLat) was 10 mm lateral to the more medial posterior meniscal insertion (MM_PostMeniscMed) (Fig. 21). The tibial insertions of all of the coronary attachments of the medial meniscus were directly inferior to their respective meniscal attachments on the medial rim of the tibial plateau.
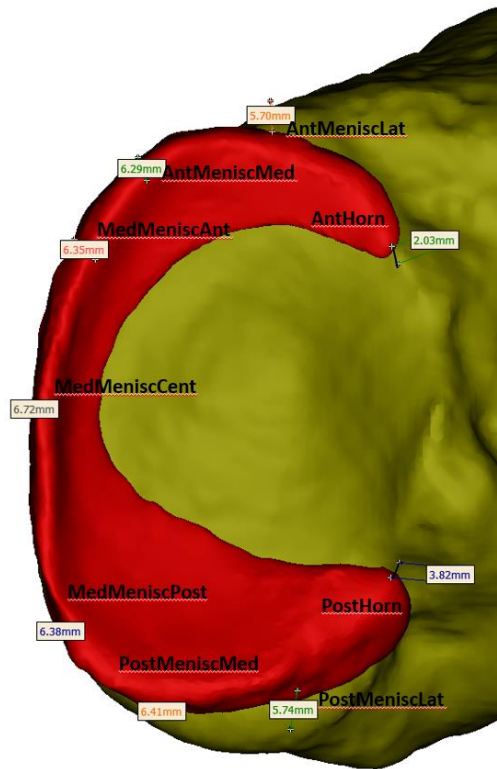
Fig. 21: Nine fibers simulating the coronary attachment of the medial meniscus, which connect the medial meniscus to the medial rim of the tibial plateau

Smoothing meniscus and cartilage

Smooth the femoral, tibial, and patellar cartilages and the meniscus geometries using Geomagic Studio. Smooth all the geometries to reduce local inconsistencies (e.g., spikes) but maintaining the overall shape of the geometry. The main steps that are applied to smooth the menisci and cartilage geometries are similar and are described below.

Meniscus

1) Use the 'Remove Spikes' feature after selecting all the polygons with a setting of 32% to 40% (Fig. 22). This command removes the spike based on a non-linear formula and we allow a volume reduction < 4% in all geometries.
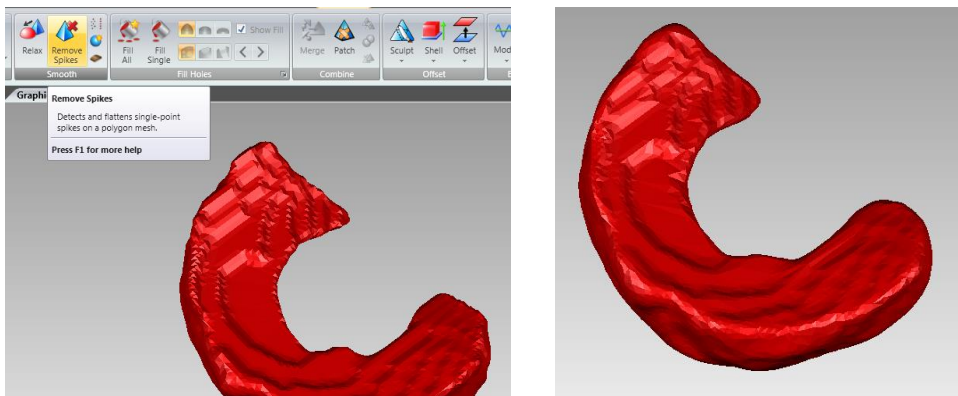
Fig. 22: Removing spikes from meniscus geometry in Geomagic

2) Use the 'Relax' feature and relax all the polygons by smoothness level of 5 (Fig. 23)
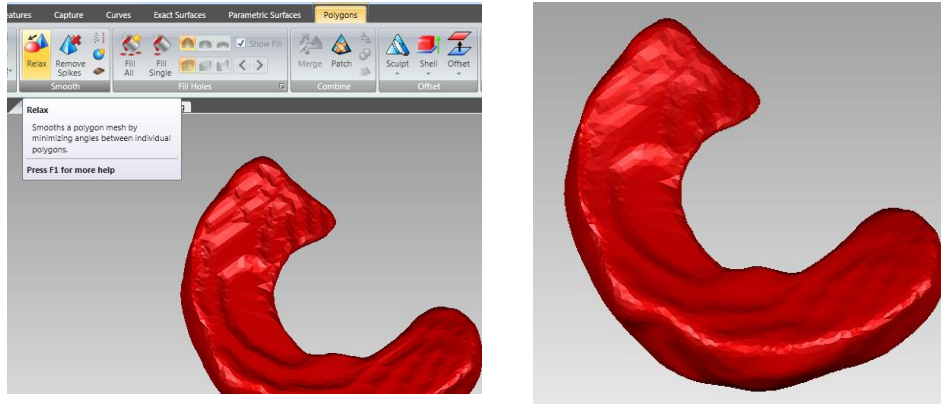
Fig. 23: Relax the angles between individual polygons in Geomagic

3) Use the 'Reduce noise' feature with smoothness level 1 and with 2 or 3 iterations for all the polygons (level 2, iteration 3) (Fig. 24)
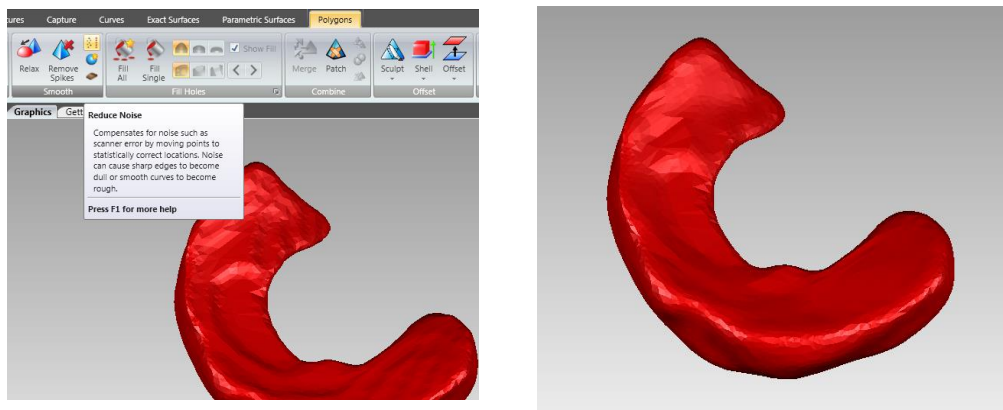
Fig. 24: Reducing noise in Geomagic

4) If there are still inconsistencies on the surface which will be in contact with another surface, only select those specific areas using the 'lasso' selection tools and relax them by smoothness level of 8 to10 and increase the strength level from 5 to 10 (Fig. 25).

32
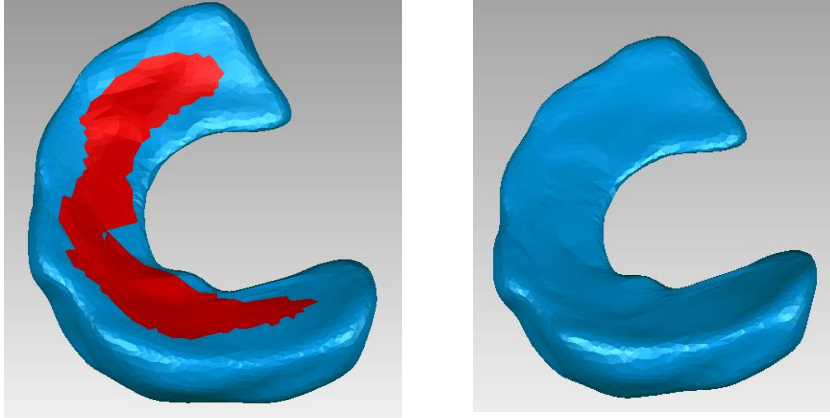
Fig. 25: Smoothing selected inconsistent surfaces in Geomagic

If the geometry still has local inconsistencies such as spikes or bumps, do the following:

5) Select the redefined icon and select subdivision 3 to increase the surface elements (Fig. 26).
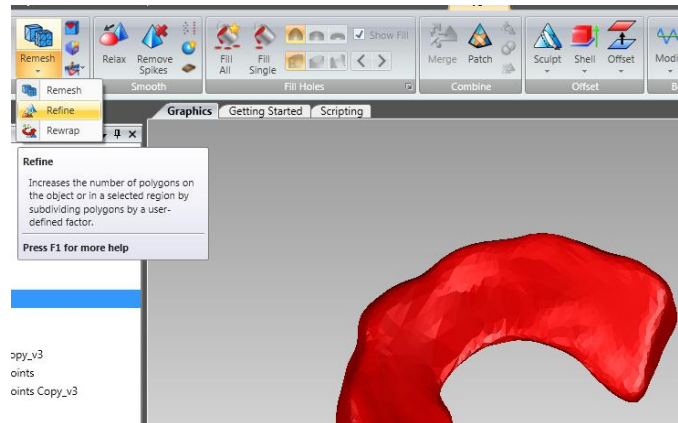
Fig. 26: Increasing the surface elements in Geomagic

6) If still has local inconsistencies, repeat steps two, three, and four. Altogeher, the meniscal geometries will have no apparent step-offs or spikes after the smoothing process is completed with < 4% change in volume of the object (Fig. 27).
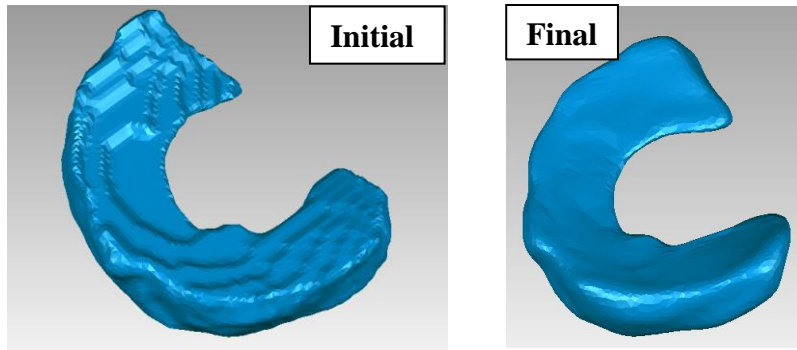
Fig. 27: Meniscus before (Initial) and after (Final) smoothing in Geomagic

After smoothing all the parts and transferring them to the femoral coordinate system (see Coordinate System Definition section), visually inspect the penetration between the meniscus and the tibia cartilages. If there is a noticeable penetration > 0.7 mm, the dynamic simulation in ADAMS may not converge or simulation time will increase. To fix this issue, move the meniscus proximally to eliminate the penetration. For example, may be a noticeable penetration between the medial meniscus and the tibial plateau at the initial position (Fig. 28). To minimize the penetration, use the 'Object Move' command in Geomagic, which can be selected from the Tools Tab. Select the meniscus and move it proximally until the penetration is visually removed.
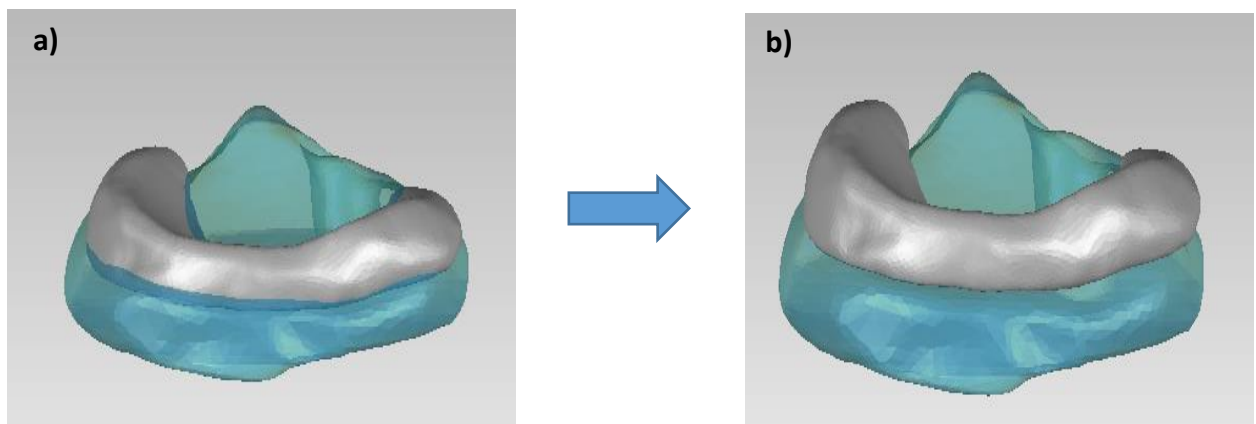
Fig. 28: a) An example of visual penetration between the meniscus and the tibial cartilage; b) the penetration was minimized by translating the meniscus proximally.

34

For the femoral cartilage, split it into two parts: medial femoral cartilage and lateral femoral cartilage as shown in Fig. 29 by using the 'Trim with plane' feature in Geomagic. Splitting the femoral cartilage will allow the medial and lateral contact forces to be measured independently.
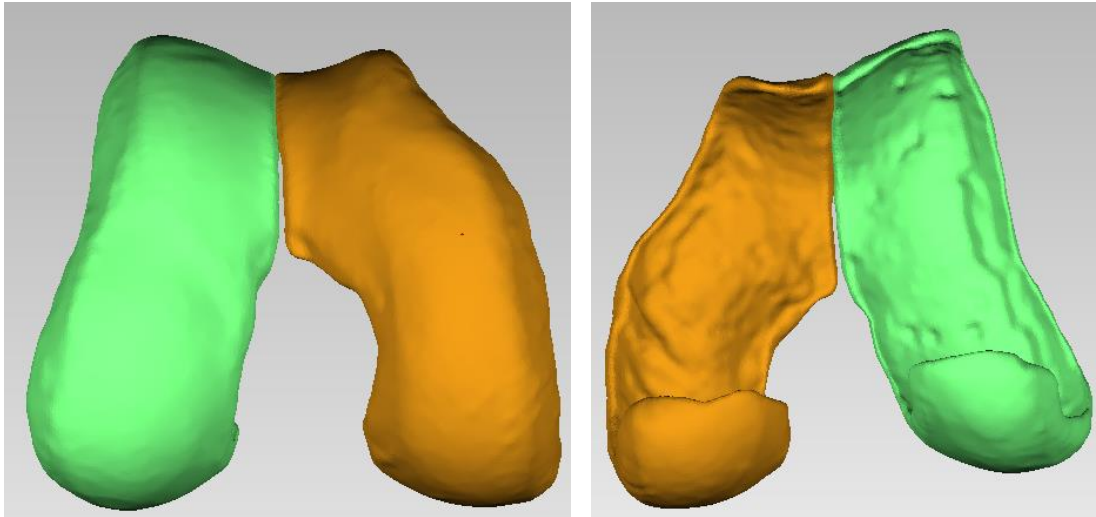

Fig. 29: Splitting the femoral cartilage into medial and lateral parts

Now, save the tibial, femoral, and patellar cartilages and meniscus as ASCII STL files.

Patellofemoral joint

The model of the patellofemoral joint consists of the patella, patellar cartilage, patellar tendon, lateral and medial patellofemoral ligaments (LPFL and MPFL), and the line of action of the quadriceps muscles.

Model the LPFL and MPFL with three tension-only linear springs each (for a total of 6 fibers). Model the patellar tendon as three tension-only springs. Define the stiffness of MPFL as 42.5 N/mm in accordance with (Criscenti, De Maria et al. 2016), the stiffness of LPFL as 16 N/mm in accordance with Merican et al. (Merican, Sanghavi et al. 2009), and the stiffness of the patellar tendon is equal to 260 N/mm as reported by Haut et al. (Haut and Haut 1997). Define the force-elongation relationship of all these ligaments as a generic-piece wise function. This relationship is detailed later in the sections of the ligament forces and slack length definition.

 Model the insertions of the MPFL as reported by Amis et al. (Amis, Firer et al. 2003), where the femoral insertions were at the medial epicondyle of the femur (very close to the femoral insertion of the sMCL) and the patellar insertions were at the medial border of the patella. The insertions of the MPFL were modeled as reported by Merican et al. (Merican, Sanghavi et al. 2009), where the femoral insertions were anchored at the proximity of the lateral epicondyle of the femur (very close to the femoral insertion of the sMCL) and the patellar insertions were at the lateral border of the patella. The insertions of the patella tendon (PT) were modeled as reported by Basso et al. (Basso, Johnson et al. 2001), where the patellar insertion were at the distal margin of the patellar apex and the tibial insertion were at the superior facet of tibial tuberosity (about 25 mm distal to the tibial articular surface).

Define three groups of muscles and subject them to constant forces as described by Beidokhti et al. (Beidokhti, Janssen et al. 2017): rectus femoris, vastus medialis and grouped vastus lateralis and intermedius. Model each muscle group by one force element. Subject the springs to constant loads of 20, 10 and 10 N, respectively, to maintain tension in the patella tendon.

Model the contact between the patella cartilage and the cartilage for the medial and lateral halves of the femoral cartilage by using the ADAMS default IMPACT function. This algorithm generates contact force as a non-linear function of penetration depth and penetration velocity at the locations

where contact is detected between rigid bodies. The contact parameters were defined according to the following relationship:

$$F = K (x)^e + B (x) * \dot{x}$$

Where K=250 N/mm and represents the stiffness, x is the interpenetration depth of geometries, e=2.2, and B= 6 N.s/mm and represent the damping coefficient, and $\dot{x}$ is the interpenetration velocity (Guess, Thiagarajan et al. 2010).

Coordinate system definitions

Define fixed coordinate systems (CS) for both the proximal tibia and the distal femur as follows. For the femur CS (FemCS), the Y-axis, which defined flexion-extension, is the line that connects the medial sulcus to the lateral epicondyle (transepicondylar axis). Align the X-axis to the long axis of the femur. Define the long axis as a line connecting the center of the cross-section of the most proximal aspect of the femur, that is available in the MRI scan, and the point that bisects the TEA. The Z-axis is the common perpendicular of the X-axis and the Y-axis (Fig. 30) .It is automatically calculated in the next steps. Use the 'Create Coordinate System by Definition' tool in Geomagic to create the FemCS. Geomagic automatically calculates the transformation matrix from the world CS (MRI CS) to the femoral CS. To export this transformation matrix, select the femur and go to Tools→Transform→Save. Add a file name and save the matrix as the transformation from SCN to Femur CS (SCN2FemCS).
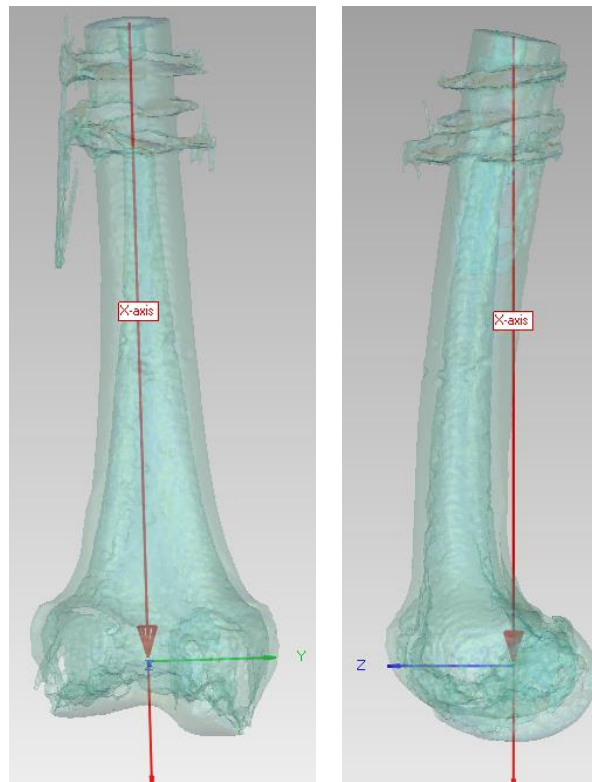
Fig. 30: the femoral coordinate system (FemCS)

in the frontal and sagittal views

For the tibia, compute the long axis (X-axis) via principal component analysis (PCA). PCA identifies the direction of most variance in the point data describing the proximal tibia, which align with the tibial long axis. Next, define the medial-lateral (ML) and anterior-posterior (AP) axes of the tibial coordinate system using the most contoured ellipse, which has the largest sum of major and minor axes lengths. Serially fitting an ellipse to axial slices perpendicular to the long axis of the tibia in 0.3 mm increments to identify the most contoured ellipse. Set the major and minor axes of the most contoured ellipse as the respective ML (Y-axis) and AP (Z-axis) axes of the tibial coordinate system; define the center of this ellipse as the origin of the tibial coordinate system (Fig. 31) (more details can be found in our publication (Amirtharaj, Hardy et al. 2018)). Then, use the 'Create Coordinate System by Definition' function in Geomagic. Export the transformation matrix from Geomagic by selecting the femur, then select Tools→Transform→Save. Add a file name and save the matrix as the transformation from SCN to tibia CS (SCN2TibCS).
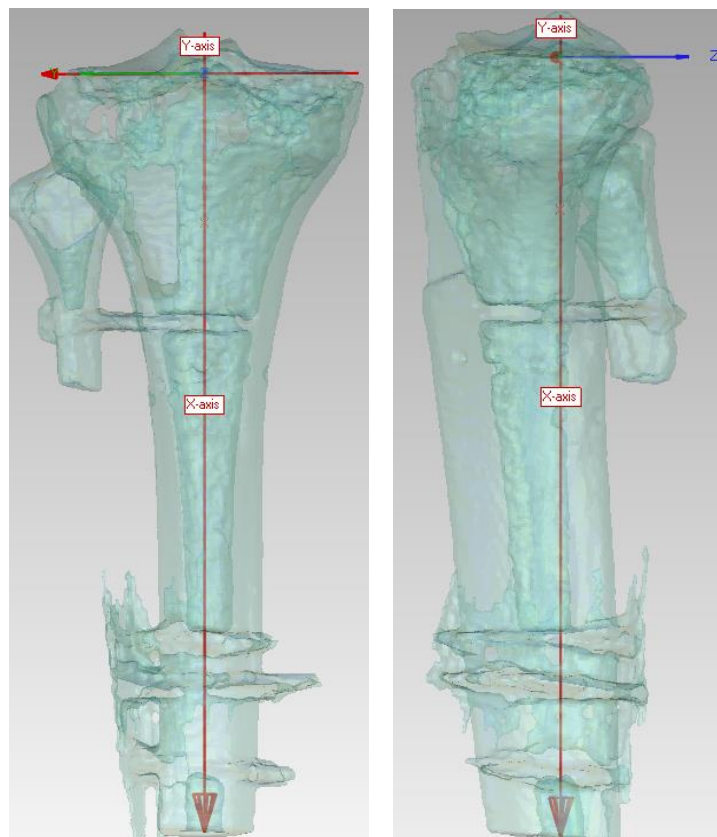

Fig. 31: The tibial coordinate system (TibCS) in the frontal and sagittal view

Finally, transform the tibia, the cartilages, and the menisci from the SCN CS to the femoral CS by using the transformation SCN2FemCS. Select each of these geometries in Geomagic; then go to 'Tools'→ Transform→ Load the SCN2FemCS file.

Define the joint coordinate system of the knee in ADAMS, which is adapted from that of Grood and Suntay (Grood and Suntay 1983); define the medial-lateral axis of the femur as the flexion-extension axis (described above) and the superior-inferior axis of the tibia (tibial long axis) as the axis to describe internal-external rotation. Finally, define the anterior-posterior axis as the common perpendicular of the femoral flexion axis and the tibial long axis.

Numerical analysis

The Automated Dynamic Analysis of Mechanical Systems software, ADAMS, is a tool for multibody dynamics simulation. ADAMS uses a predictor-corrector numerical algorithm to solve the dynamic equations based on the motion time history and current motion trajectory. This formulation is suitable in circumstances that involve rapid increases in forces due to contact, or rapid changes in bone position in response to low applied forces due to the geometric non-linearity of the articulating bone surfaces. The dynamic analysis involves developing and then integrating the non-linear ordinary differential equations of motion (Imhauser 2004).

Use Dynamic analysis (GSTIFF integrator) to solve the dynamic equations of motion describing our model (Fig. 32). Given the position of the system at time t_0, the problem was to determine the position at time $t_1 > t_0$. A Newton-Raphson method is used in ADAMS to compute the new position at time t_1. Use the following solver settings in our models: integrator error of 0.001; maximum number of iterations of 25; initial simulation step size of 0.001 s; and a step size of 0.005 s.
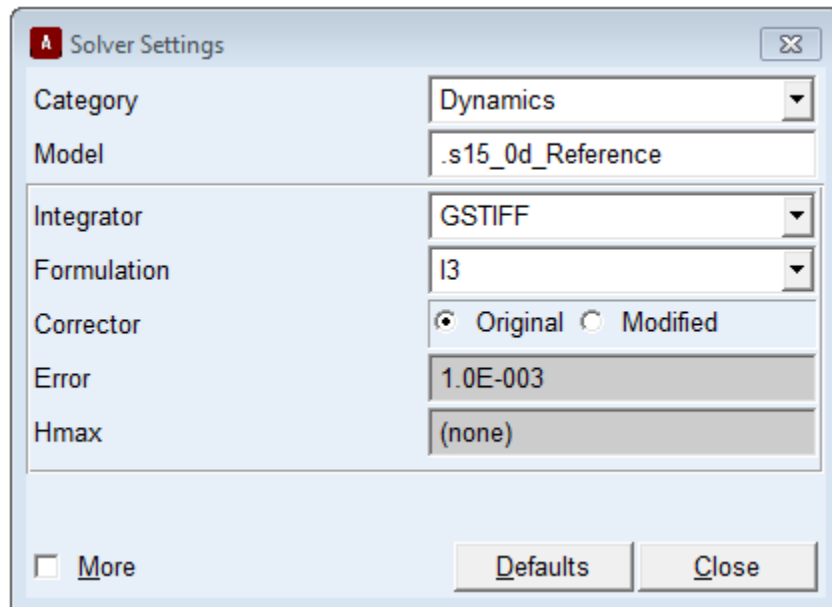

Fig. 32: The Dynamic analysis settings in ADAMS View

Assembling the model in ADAMS

First, use Geomagic to make sure that the position and orientation of all parts are decribed relative to the femoral coordinate system (FemCS). Save all the final parts of the femur, tibia, cartilage, and menisci as STL ASCII files in Geomagic. Next, begin a new database in ADAMS and import all parts into in this new database. Inspect all geometries for any missing triangles. If any triangles are missing, go back to Geomagic further refine the geometries according to the steps described in the smoothing section and export the part again. Then, export all parts as Parasolid, ASCIIi file from ADAMS-Do not use Solidworks or Geomagic for this because they reduce the smoothness of the geometry). Finally, import the Parasolid parts again into a new database in ADAMS (Fig. 33).
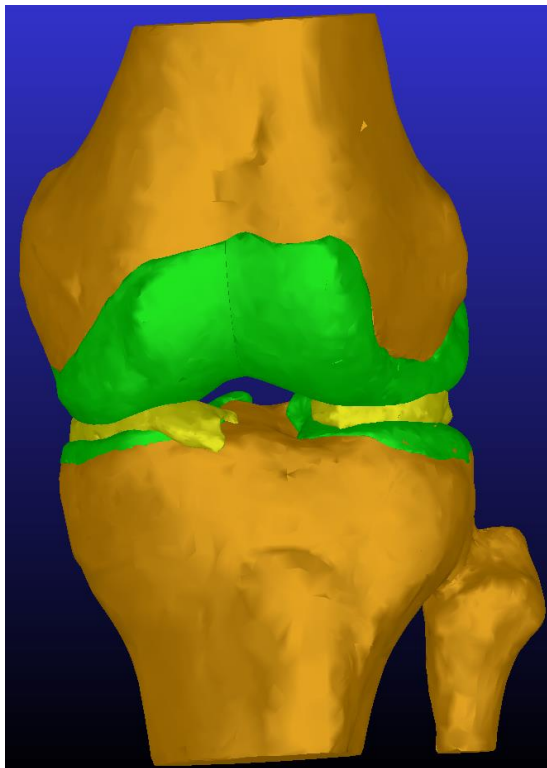
Fig. 33: Model assembly in ADAMS

Specifically, the following parts should be imported into the new database (Fig. 34).

- Femur

- Tibia

- Femoral cartilage medial

- Femoral cartilage lateral

- Tibial cartilage medial

- Tibial cartilage lateral

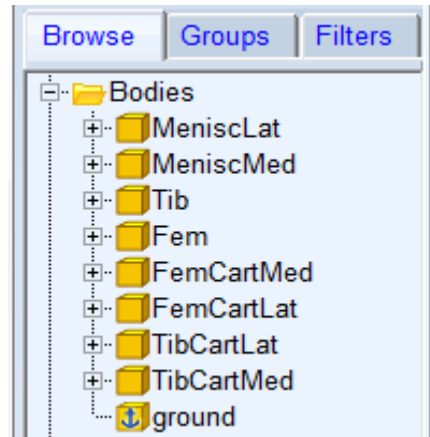- Meniscus medial

- Meniscus lateral

Fig. 34: List of parts imported to ADAMS View

Make sure the gravity option is turned 'off' and select the directory to which you would like to save ADAMS files. Finally, change the rotation sequence to "123" in ADMS via the following command: 'Settings' ☐ 'coordinate system'.

Defining mass properties, joints, and forces

In this portion of the workflow, incorporate the transformation matrices (SCN2FemCS and SCN2TibCS) and ligament insertion files as inputs to a Matlab script developed by our research group. The script produces a .cmd file, which is a text file in the ADAMS command language that we use to define all structural properties, loading conditions, joints between parts, coordinate system definitions, as well as model outputs (e.g., kinematics, ligament forces, contact forces, etc.) in ADAMS. We can also define measures, sensors, and variables depending on the objective of the simulation by using Matlab macros. All of these definitions can also be directly defined in the ADAMS View software as summarized below.

1- Mass properties of bones, cartilage, and meniscus

Define all bone and cartilage geometries as rigid bodies with densities of 1600 kg/m3 and 1000 kg/m^3, respectively. At this stage of the workflow, define both menisci as rigid bodies with a density of 438 kg/m^3. This definition, however, will be changed in subsequent steps when we discretize the meniscus.

In the ADAMS View software, define the mass properties of the tibia (and all model geometries) as shown in Fig. 35. Note that these values can also be stored as design variables in ADAMS, to parametrically study the effect of a variable on the model outputs. Either enter the actual numerical value for density directly or as a design variable.
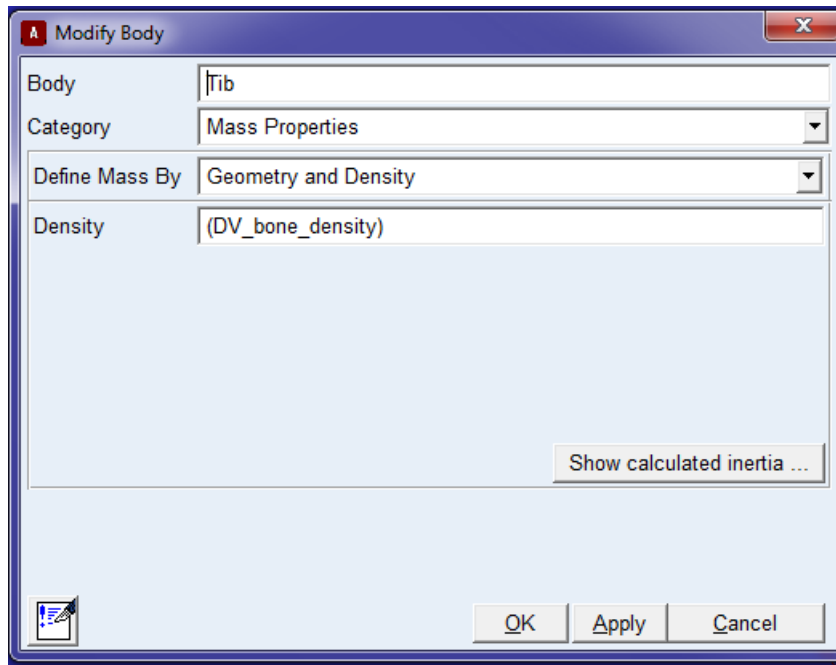
Fig. 35: Defining mass properties of the tibia in ADAMS View. In the 'Density' input line under the 'Modify Body' command, the name, 'DV_bone_density' had been entered. This is a design variable that contains the actual value, but can also be parameterized over a range of values for sensitivity analysis.

2- Joints

Define the following joints (i.e., constraints) between the model parts. These joints rigidly constrain cartilage to bone geometries.

a) A fixed joint (i.e., zero degrees of freedom) between lateral femoral cartilage and femur
   Location: 0,0,0
   Orientation: 0,0,0

b) A fixed joint between medial femoral cartilage and femur
   Location: 0,0,0
   Orientation: 0,0,0

c) A fixed joint between lateral tibial cartilage and tibia
   Location: 0,0,0
   Orientation: 0,0,0

d) A fixed joint between medial tibial cartilage and tibia

Location: 0,0,0

Orientation: 0,0,0

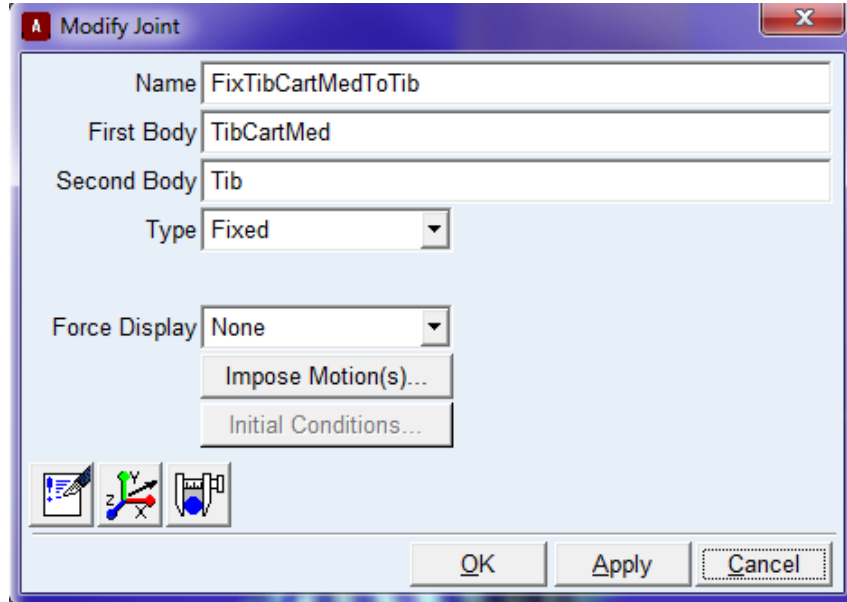An example of how we defined a fixed joint in ADAMS (Fig. 35):

Fig. 36: Example of defining a fixed joint in ADAMS View between the medial cartilage of the tibia (First Body: TibCartMed) and the Tibia (Second Body: Tib).

3- Forces

Ligament forces:

Define the force-elongation response curves of the 45 fibers representing 13 different ligaments in ADAMS View. Represent fibers with straight-line force elements between their two insertions Define each ligament fiber in ADAMS as a 'single-component force'. Describe the structural properties of each ligament fiber using a tension-only, non-linear force-elongation relationship (Eqs. 1a, b),

$$F(l, \dot{l}, l_0) = \frac{1}{n}\{[f^*(l) + c_d \dot{l} B_1]B_2 + [K(l - (l_0 + \Delta_t)) + f^*(l_0 + \Delta_t) + c_d \dot{l} B_1]B_3\} \tag{1a}$$

$$B_1 = step(\dot{l}, 0, 0, \dot{l} + 0.1, 1)$$

$$B_2 = step(l, l_0, 0, l_0 + 0.1, 1) \times step(l, (l_0 + \varDelta_t), 1, (l_0 + \varDelta_t) + 0.001, 0) \qquad (1b)$$

$$B_3 = step(l, (l_0 + \varDelta_t), 0, (l_0 + \varDelta_t) + 0.001, 1)$$

where n is based on the number of fibers and their arrangement, l is the inter-insertional distance, $\dot{l}$ is the first derivative of the inter-insertional distance with respect to time, and l_0 is the ligament slack length. $f^*(l)$ is a spline representing the toe region of the ligament force-elongation response. It was obtained by directly digitizing plots of the ligament force–elongation response from the literature (Butler, Guan et al. 1992; Robinson, Bull et al. 2005; Hauch, Villegas et al. 2010; Wilson, Deakin et al. 2012). We observed that the toe region varies in shape from ligament to ligament so we chose to include representations that were more specific to individual ligaments. The AKISPL spline function available in ADAMS View was used. This function uses Akima interpolation, which provides estimates for the first derivative of the approximated function when the data points are evenly spaced. K represents the linear portion of the force-displacement response. The transition between the toe region and linear region is defined by $\varDelta_t$. Each force element also included a parallel damping term ($c_d = 1.5$ Ns/mm) based on the stress relaxation response of ligaments (Funk, Hall et al. 2000). The step functions B_1, B_2, and B_3 are cubic polynomials that allow continuous and smooth generation of tensile forces as a ligament fiber becomes taut.

Define the location-dependent structural properties of the AM, AL, and PL groups of the ACL based on the work of (Butler, Guan et al. 1992). Assume the structural properties of the ALL to be half of the LCL based on the observation that the ALL is thinner and less stout than the LCL. Describe the structural properties of the posterior capsule using a cubic spline that fit the properties of the sMCL (Robinson, Bull et al. 2005) since both have a stout appearance based on visual inspection. Model the horn attachments of the menisci with a linear tension-only force-elongation response and stiffness of 180 N/mm (Hauch, Villegas et al. 2010). Model the tibiomeniscal coronary ligaments as tension-only linear springs on the medial and lateral side with a stiffness about half that of the sMCL (90 N/mm) based on its relatively loose connection to the proximal tibia observed by direct visualization during cadaveric dissections by our research group. Do not

model the transverse intermeniscal ligament due to its non-stout appearance in our cadaveric dissection work. The structure properties of the ligament are summarized in Table 1.

For example, define the force generated in a single fiber (in this case of the OPL) in ADAMS View as follows (Fig. 37):
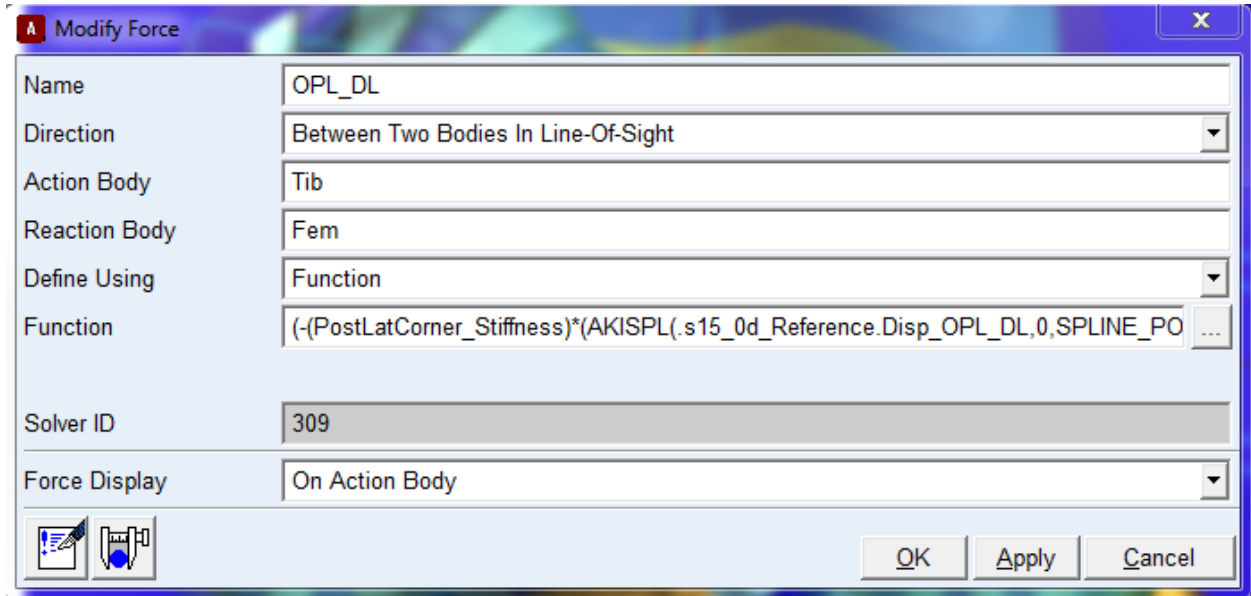

Fig. 37: A sample of how the ligament formula is written in ADAMS View (for the OPL in this case)

Table 1: Structure properties of the ligaments used in the model

Ligament	K (N/mm)	Reference of spline for toe region
ACL_1,3	19.09	(Butler, Guan et al. 1992)
ACL_2	25.4	(Butler, Guan et al. 1992)
ACL_4,5,6	28.78	(Butler, Guan et al. 1992)
PCL_1,2,3,4	57	(Harner, Xerogeanes et al. 1995)
PCL_5,6,7	120	(Harner, Xerogeanes et al. 1995)
MPC*	-	(Robinson, Bull et al. 2005)
LPC*	-	(Robinson, Bull et al. 2005)
OPL*	-	Same as POL
FFL*	-	Same as POL
LCL	59	(Wilson, Deakin et al. 2012)

ALL	30	(Wilson, Deakin et al. 2012)
POL	56	(Robinson, Bull et al. 2005)
sMCL	80	(Robinson, Bull et al. 2005)
LM_horn**	180	
MM_horn**	180	
LM_Coron**	36	
MM** (other)	36	
*	B3= 0 in equation 1a	
**	f*(l)= 0, B2= 0, B3= step (l, l$_0$, 0, l$_0$ +0.1, 1)	

Contact forces:

Model cartilage-cartilage contact and menisci-cartilage contact using the ADAMS default IMPACT function. This algorithm generates contact force as a non-linear function of penetration depth and penetration velocity at the locations where contact is detected between rigid bodies. The algorithm does not provide predictions of contact stress. The contact forces and kinematics that develop from this contact algorithm, however, depend on the shape of the articular and meniscal restraints. Therefore, the algorithm is useful for predicting knee mechanics on a subject-specific basis, which is a focus of our research group.

The contact forces were defined according to the following relationship:

$F = K (x)^e + B (x) * \dot{x}$

Where K=250 N/mm (for cartilage-cartilage contact) and K= 10 N/mm (for cartilage-meniscus contact) and represent the stiffness. These properties were chosen primarily based on the work of Guess et al. who calibrated these properties based on linear finite element analysis (Guess, Thiagarajan et al. 2010). For the other properties, similar values are defined in cartilage-cartilage contact and in cartilage-meniscus contact. Specifically, x is the interpenetration depth of geometries, e=2.2, and B= 6 Ns/mm and represent the damping coefficient, and $\dot{x}$ is the interpenetration velocity.

Define seven contact forces between the following pairs of geometries:

a) medial tibial cartilage and medial femoral cartilage

b) lateral tibial cartilage and lateral femoral cartilage

c) medial meniscus and medial femoral cartilage

d) lateral meniscus and lateral femoral cartilage

e) medial meniscus and femur

f) lateral meniscus and femur

g) tibia and femur

An example of a contact force created between the lateral meniscus and lateral femoral cartilage in ADAMS Views is shown in Fig. 38:
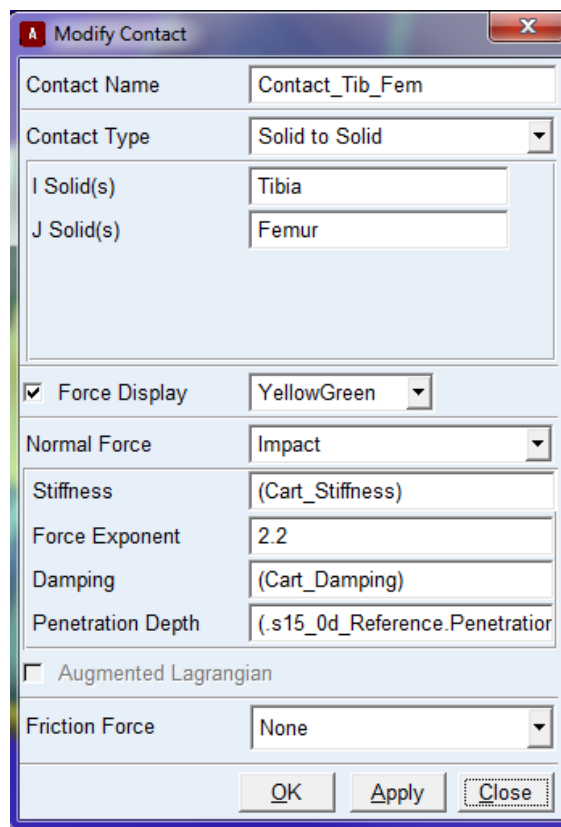

Fig. 38: An example of defining a contact force between Tibia (I Solid) and Femur (J Solid) in ADAMS View

External forces: Define several commonly-used external forces when developing the model as single-component forces; activate/deactivate them according to the objective of the simulation. Typically, assign each force to be 'Moving with body' so that the force can track the bone as it moves in 3D space (Fig. 39).

50

a) Compression force (ForceCD): A compression force applied along the long axis (X-axis) of the tibia

b) Anterior-posterior force (ForceAP): anterior-posterior force applied along the common perpendicular of the flexion axis of the femur and the long axis of the tibia.

c) Varus/valgus Moment (MomVV): A rotational force that rotates the tibia about the common perpendicular of the flexion axis of the femur and the long axis of the tibia

d) Internal/external Rotation Moment (MomIE): A rotational force that rotates the tibia long axis.

See Fig. 39 for an example of the how a force or moment is defined in ADAMS View:
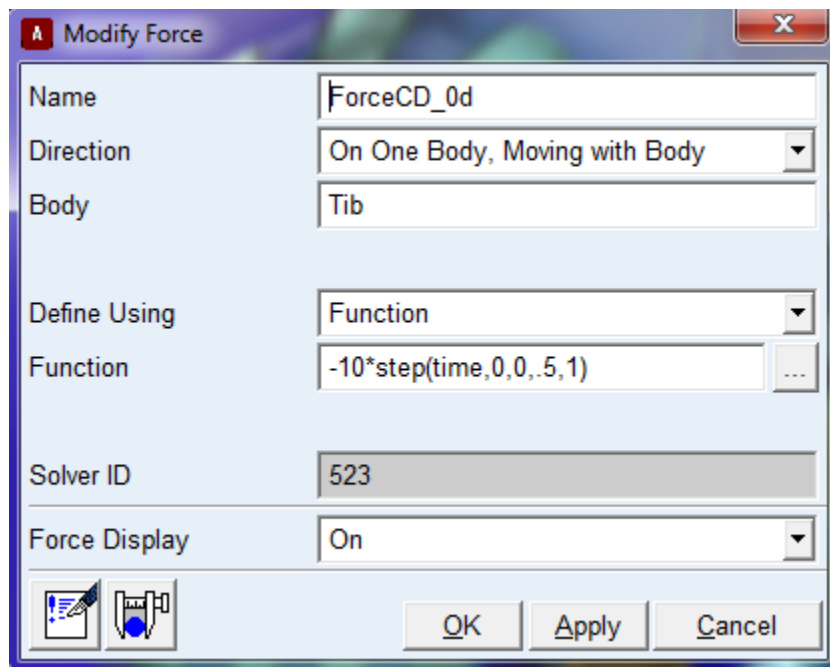
Fig. 39: An example of how external forces were defined in ADAMS. In this case, a compression force applied on the tibia

Meniscus discretization

Discretize the lateral and medial meniscal geometries radially and connect each element with a 3D spring following the method of Guess et al. (Guess, Thiagarajan et al. 2010). Altogether, this approach provided a deformable representation of the menisci in the multibody dynamics framework in which the lateral and medial meniscal geometries were divided into 34 and 31 segments, respectively (Fig. 40).
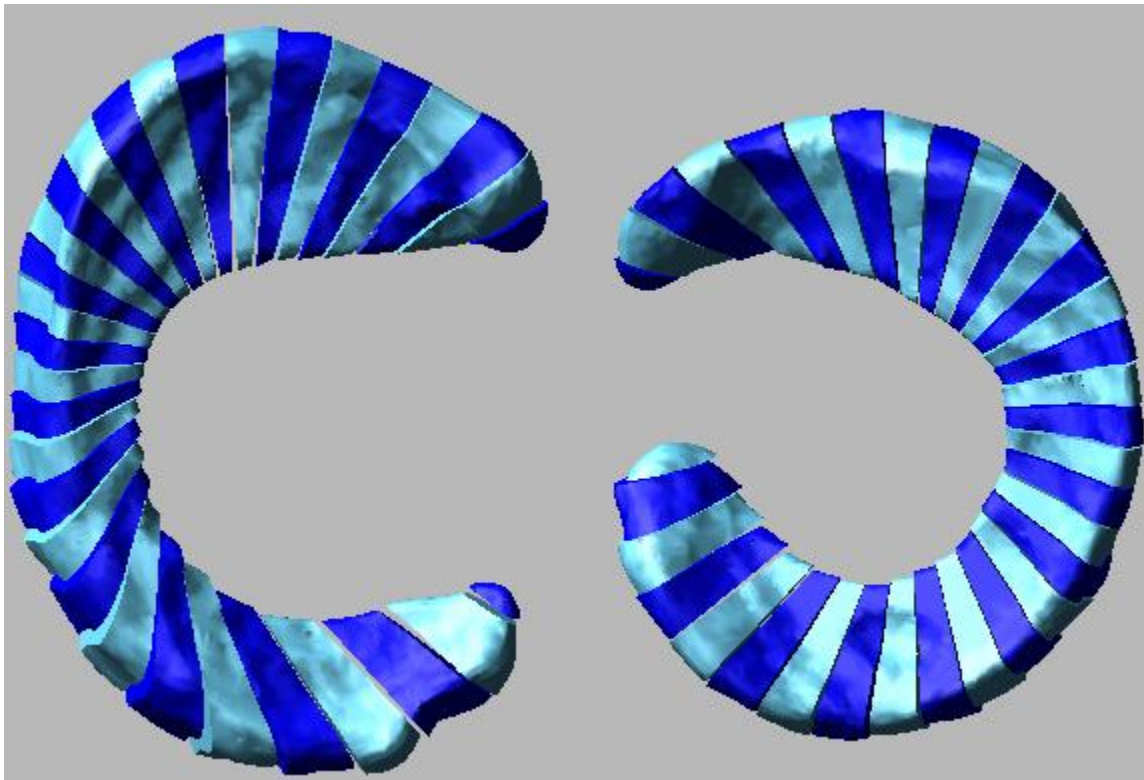

Fig. 40: Discretized medial (right) and lateral (left)

Connect each wedge-shaped section to the adjacent section by defining the following stiffness matrix:

$$\begin{bmatrix} Fx \\ Fy \\ Fz \\ Tx \\ Ty \\ Tz \end{bmatrix} = \begin{bmatrix} Kxx & Kxy & Kxz & 0 & 0 & 0 \\ Kxy & Kyy & Kyz & 0 & 0 & 0 \\ Kxz & Kyz & Kzz & 0 & 0 & 0 \\ 0 & 0 & 0 & Txx & 0 & 0 \\ 0 & 0 & 0 & 0 & Tyy & 0 \\ 0 & 0 & 0 & 0 & 0 & Tzz \end{bmatrix} \begin{bmatrix} x \\ y \\ z \\ a \\ b \\ c \end{bmatrix}$$

Where $F_{x,y,z}$ and $T_{x,y,z}$ are the forces and torques between elements acting in the circumferential (x), radial (y), and axial directions (z). K_{xx}, K_{yy}, K_{zz}, K_{xy}, K_{xz}, K_{yz}, T_{xx}, T_{xy}, and T_{xz} are the stiffness matrix parameters, x, y, and z are relative translational displacements and a, b, and c are relative rotations. The same stiffness matrix parameters were used to connect each element of both the medial or lateral meniscus (Guess, Thiagarajan et al. 2010). These parameters incorporating circumferential, radial, and proximal-distal terms, were calibrated from a linear, transverse, isotropic finite element formulation to represent a deformable geometry (Guess, Thiagarajan et al. 2010)

Modeling steps:

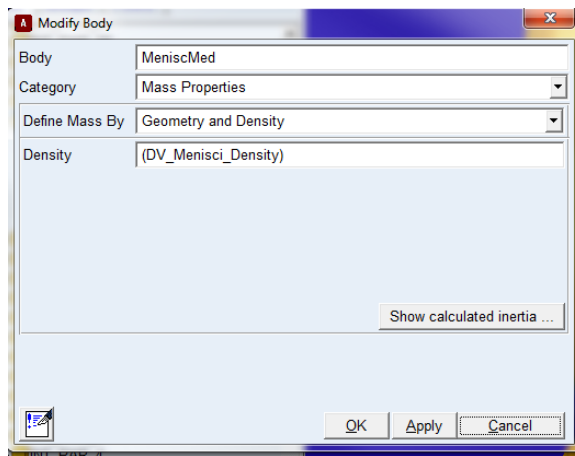1- Define the meniscus density equal to 10^{-5} kg/m^3 in ADAMS View(Fig. 41)

Fig. 41: Meniscus density updated to 10^{-5} kg/m^3. This values is stored in the design variable: DV_Menisci_Density

2- Change coordinate system setting from '123' to '313' settings in ADAMS View (Fig. 42). The 313 rotation sequence method represents successive rotations of Euler angles around the Z-axis, then the new X-axis, then the new Z-axis.
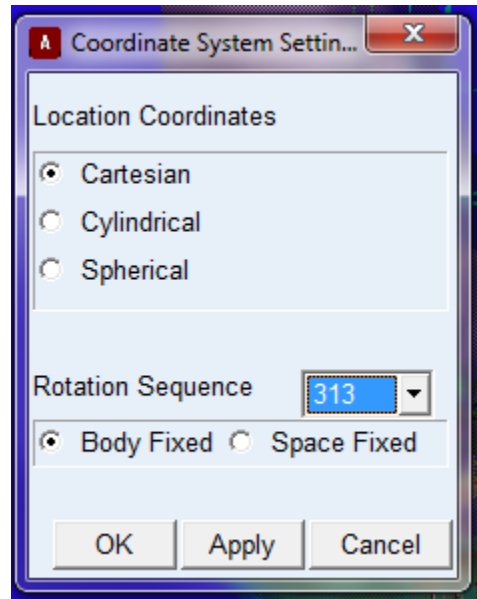

Fig. 42: Changing the coordinate system setting to '313'

3- Divide each meniscus into multiple wedge-shaped elements

In this step, circumferentially divide each meniscus into smaller, wedge-shaped elements that will subsequently be connected with 3D spring elements. To do so, apply the following steps for each meniscus separately; we show the lateral meniscus as an example:

a- Create a cylinder in ADAMS View that occupies the inner circle of the lateral meniscus. The center of the cylinder is usually 3 mm medially from the meniscus center of mass in the YZ plane (axial plane). The cylinder height must exceed the meniscus thickness. We usually set the upper and lower boundaries of the cylinder from -100 to 100 mm along the X-axis. Set the radius of the cylinder according to the size of the meniscus and to be no more than the inner radius of the meniscus (Fig. 43).
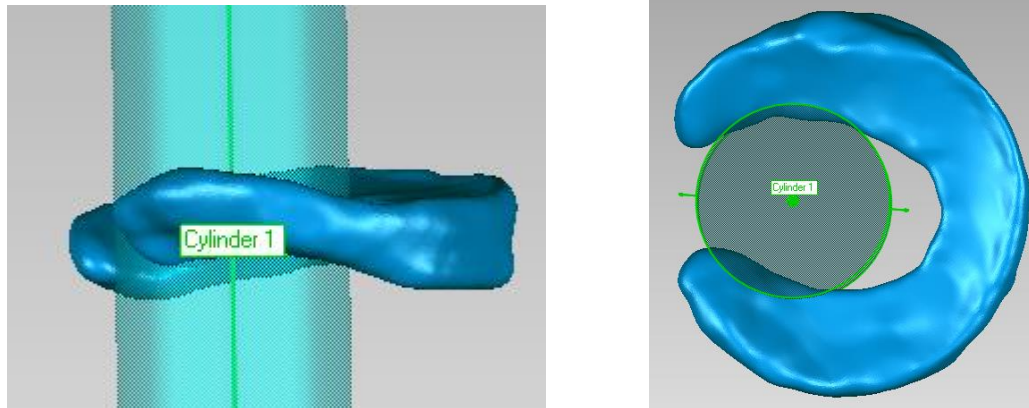
Fig. 43: A cylinder that occupies the inner radius of the lateral meniscus

b- Make a copy of the geometry of the lateral meniscus

c- Define planes around the long axis of the cylinder that is 10° apart from each other (you may change the 10° parameter to have bigger/smaller elements). An angle of 10° provides wedges that are adequate to represent the deformable meniscal geometry, but still allow relatively short simulation times. The intersection between these planes and the geometry of the lateral meniscus will define the geometry for each element. Usually, we divide the lateral meniscus into 31 elements (Fig. 44).
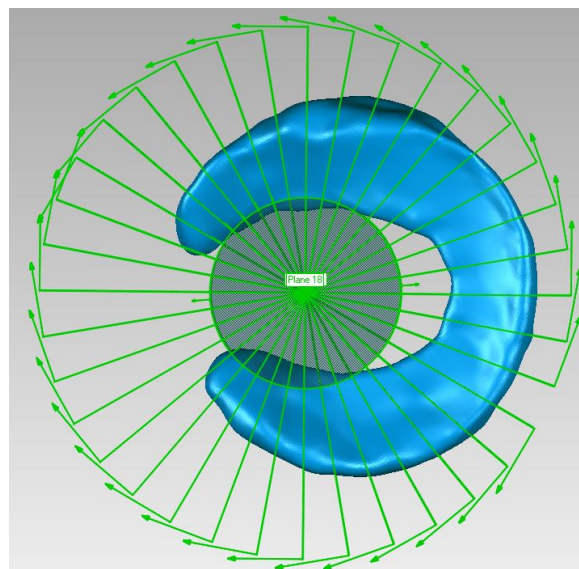
Fig. 44: Planes rotated about the long axis of the cylinder in 10° increments

d- Define a new part for each meniscus element.

e- Apply alternating colors to each meniscus element giving a checkerboard appearance to the deformable meniscus representation (Fig. 45). This differentiates the deformable meniscus representation from the rigid body formulation.
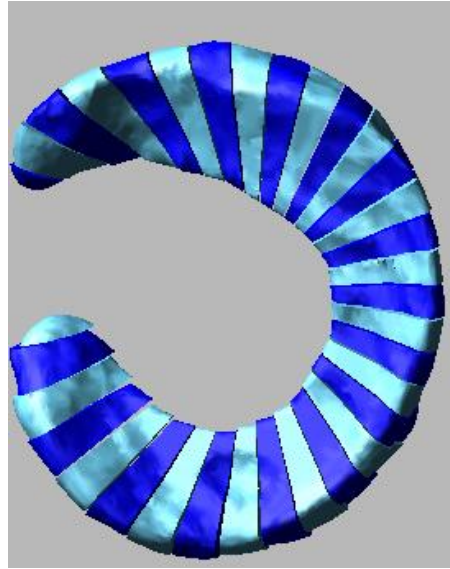

Fig. 45: Assigning to alternating colors to all meniscus elements

f- Delete the original lateral meniscus part (i.e., the rigid body)

g- Redefine the ligaments that were previously attached to the rigid body representation of the meniscus, which was just deleted in step f above (LM_PostHorn, LM_AntHorn, LM_LatCoronary for the lateral meniscus). Specifically, change the 'Action Body' in the force function of these ligaments from MeniscLat (the deleted part) to the new discretized meniscal element that is in the same location of the meniscal attachment (Fig. 46).
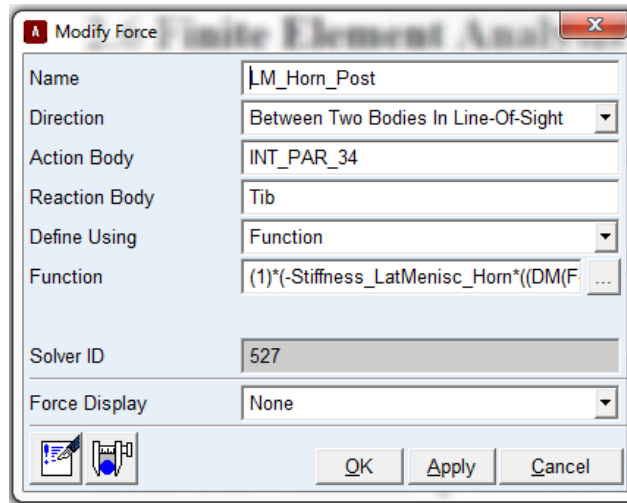
Fig. 46: Modify the 'Action Body' of the force function to attach meniscal ligaments to the discretized meniscus

Notes:

- Rename the force marker so that they are not attached to the previous solid representation of the lateral meniscus, which has now been deleted.
- Define the tibial and meniscal attachment of each horn ligament at the same point.

4- Delete the contacts between the solid representations of the lateral and medial menisci and the tibial and femoral cartilages

5- Delete any previous analyses

6- Convert all the elements of each menisci into Parasolid format

7- Assign density of 10^{-5} kg/m^3 for each segment

8- Add a field element between every two meniscal elements.

This field variable will represent a spring between every two adjacent meniscal elements. Assign the stiffness matrix described above in these field variables. The value of the stiffnesses in each direction were defined as shown in Table 2. Add each stiffness value in a separate design variable (Fig. 47).

Table 2: The stiffnesses of the springs (N/mm) between each two adjacent meniscal segments in all directions for both the medial and lateral meniscus

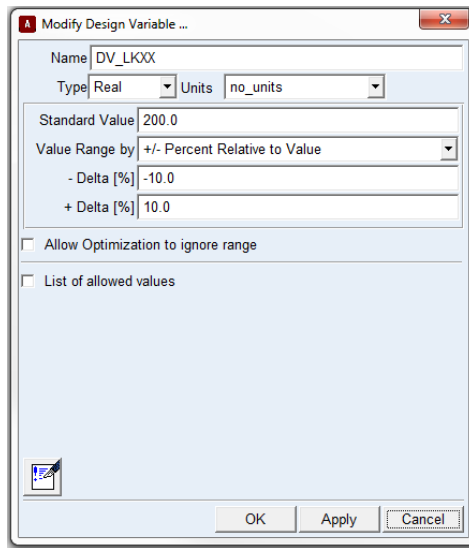|	
K_{xx}	200
K_{yy}	75
K_{zz}	75
K_{xy}	50
K_{yz}	50
K_{xz}	50
T_{xx}	25
T_{yy}	25
T_{zz}	25

Fig. 47: Defining the magnitude of the stiffness component K_{xx} in a design variable. All other stiffness components are similarly defined in ADAMS View.

9- Meniscus contacts

Define the following contacts for all the segments in the medial and lateral meniscus (Fig. 48). We developed macros that generate these contact forces in the model automatically.

    a- Contact between the medial meniscus and the tibial medial cartilage

    b- Contact between the medial meniscus and the femoral medial cartilage

c- Contact between the lateral meniscus and the tibial lateral cartilage

d- Contact between the lateral meniscus and the femoral lateral cartilage

Table 3 shows the values of the contact parameters.

Table 3: Parameters for contact of each Meniscal element and the medial tibial and femoral cartilage (for the medial meniscus) and the lateral tibial and femoral cartilage (for the lateral meniscus)

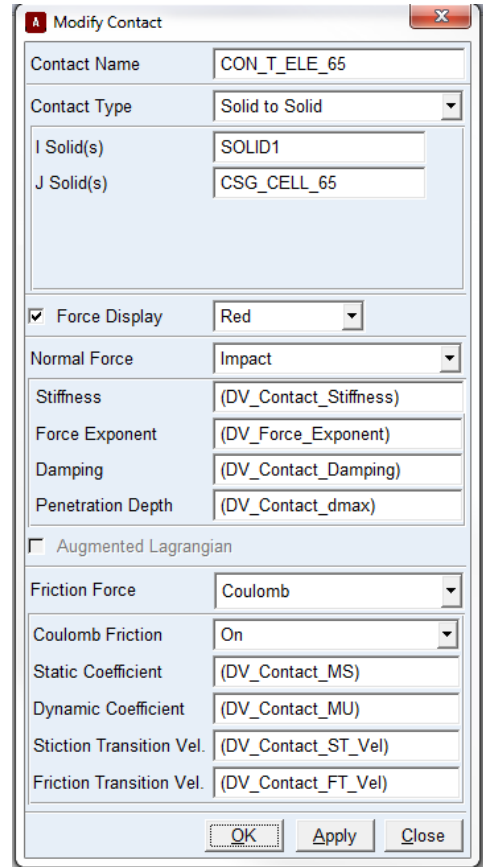| Stiffness	10.0
Force exponent	2.2
Damping	6.0
Penetration Depth	0.5
Static Coefficient	0.0
Dynamic Coefficient	0.0
Stiction Transition Vel.	100.0
Friction Transition Vel.	1000.0

Fig. 48: Defining contact between two meniscal elements in ADAMS

Contact Assessment

Conduct a contact assessment to ensure that the model has no penetration in the opposing contact surface that produces a contact force > 10 N at the initial position. For example, there could be an initial interpenetration between the meniscus elements and the femoral cartilage (Fig. 49).
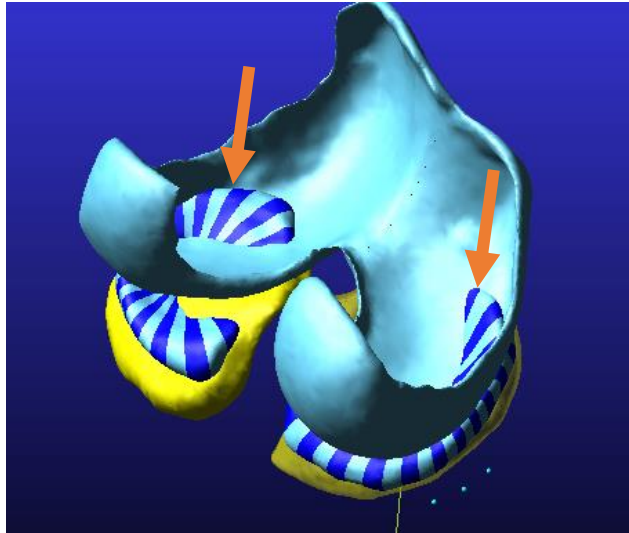

Fig. 49: Interpenetration between the meniscal elements and the femoral cartilage

1. To address this issue, deactivate the constraint that prevents the tibial flexion (FixFlex) and deactivate the fixed joint that fixes the tibia to the ground (FixTib2Ground). Next, activate the axial constraint between the femur and the tibia. Then, move the tibia distally apart from the femur (i.e., distract the tibiofemoral joint) using this equation: (8*sin(time*pi/2)). This function distracts the tibiofemoral joint by 8 mm over 1 second. Altogether, this process enables the menisci to establish a new equilibrium position that minimizes penetration between the tibial and femoral cartilage objects. Next, do the following steps:

   a. Deactivate all the contacts between al meniscal elements and tibial and femoral cartilages.

b. Run the simulation for 1 second (until all meniscus femoral cartilage penetrations were removed).

c. Make sure to deactivate the axial constraint between the femur and the tibia.

d. Reactivate the contacts between all meniscal elements and tibial and femoral cartilages and run the simulation for 1 more second.

The tibia, tibia cartilage, and meniscus all move distally by 8 mm (i.e., the tibiofemoral joint is distracted by 8 mm) during the 1st one second (i.e., the first half) of the simulation (Fig. 50) and then, during the next one second (i.e. the second half) of the simulation the tibia and its cartilage return to their initial position minimizing interpenetration between the cartilage and meniscal elements (Fig. 51).
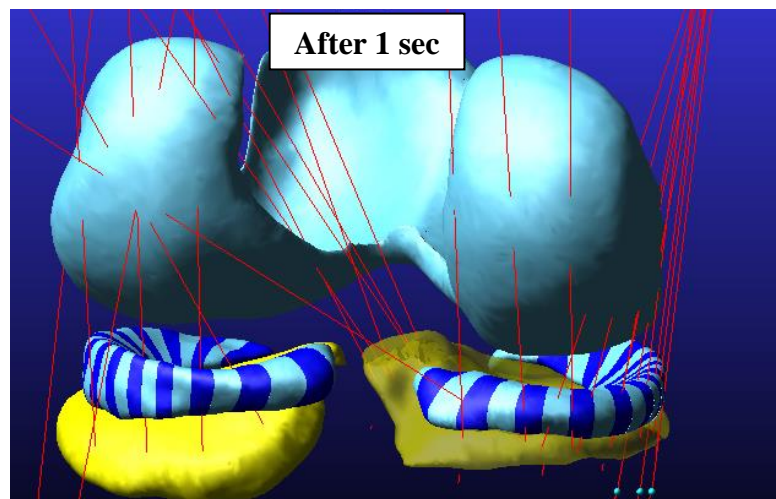

Fig. 50: In the first second of simulation, the tibia, tibia cartilage, and meniscus move distally by 8 mm
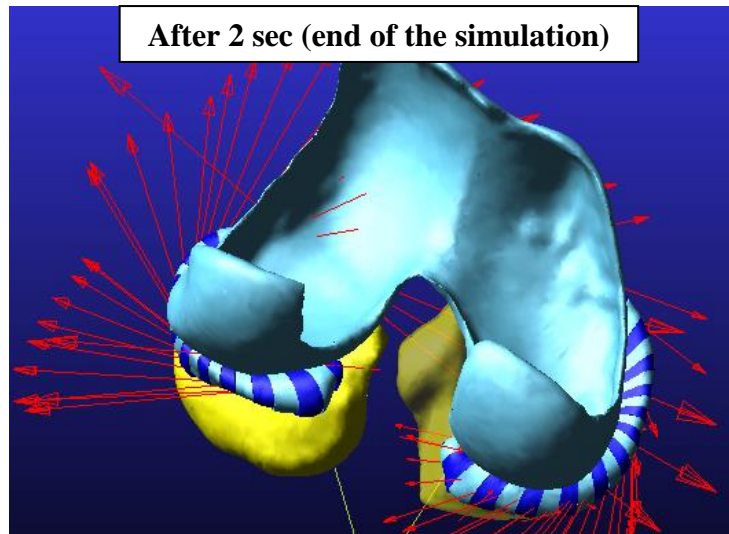
Fig. 51: In the next one second, the tibia, tibia cartilage, return to their
initial position and interpenetration between cartilage and meniscal
elements is minimized

Accordingly, all initial penetration was minimized, and the meniscus elements achieved a new equilibrium position.

2. Manually measure the distances of all the meniscal (medial and lateral) attachments (L0), measured in Mimics in the ligament mapping section, and update the design variable (L0) in ADAMS View.

3. Delete the original model version and rename the new equilibrium model with the original name.

4. If meniscus contact force is >10 N between any meniscal elements and a tibia or femoral cartilage, do the following steps below. The purpose of this procedure is to allow the meniscal elements to shift to a more conforming position around the tibial and femoral cartilage.

   a. Right click on each meniscal spring in the 'Forces' section, and select 'Modify'. Change the stiffness of springs to 1 N/mm to allow them to shift to a more conforming position with minimal penetration into the cartilage geometries.

   b. Run another simulation to enable the menisci to move to a more conforming position. Save the new menisci position by saving the model at the last frame of the simulation.

c. In this configuration, change the spring stiffnesses back to their original values.

d. Lastly, measure the distances between meniscal ligament markers, and copy and paste these values into the corresponding initial lengths (L_0's under 'Design Variables'). Delete the original version of the model, and save the modified version with the original model name.

If the menisci conform with the femoral condyles, move to the next step. If the menisci still do not conform with the femoral condyles, reposition both the menisci and the femoral condyles in Geomagic and move the menisci to create more contact penetration with the femur. Then, repeat the contact assessment in ADAMS.

MCL wrapping

Model wrap the sMCL around the proximal tibia by connecting the proximal and distal fiber groups of the sMCL with 1 mm diameter spheres located ~10 mm below the joint line (Fig. 52). Constrain each sphere tangent to the proximal surface of the tibia via a planar joint andwithin this plane using a linear spring. Assign this spring a stiffness ten times less than that of the sMCL (5 N/mm) based on the weak connection that we observed between the sMCL and the proximal tibia while dissecting cadaveric knees in our laboratory. The anterior and posterior spheres were also linked to the central sphere with a linear spring to simulate the transverse properties of the sMCL (Quapp and Weiss 1998) .
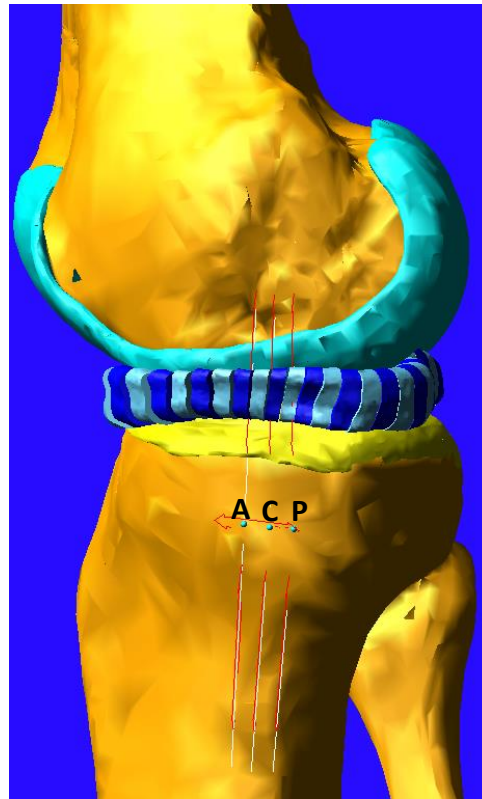

Fig. 52: MCL wrapping about the medial aspect of the tibia via anterior (A), central (C), and posterior (P) spheres restrained to the proximal tibia

A Matlab script is used to automatically accomplish the steps summarized above to model sMCL wrapping. The script executes the following steps:

1- Create three small (1 mm diameter) rigid spheres located anteriorly (A), centrally (C), and posteriorly (P) on the proximal tibia ~10 mm below the joint line. Position them as shown

in Fig. 52. The row of spheres is located~10 mm below the joint line. The anterior and posterior spheres are located about 8 mm apart from each other covering the width of the sMCL (Liu, Yue et al. 2010); the central sphere is located midway between the anterior and posterior spheres. The set of three spheres is also positioned directly distal to the proximal insertion of the sMCL (Fig. 52).

2- Define the mass of each sphere to be 0.001 kg (Fig. 53). This mass was chosen to be small to minimize their inertial effects.
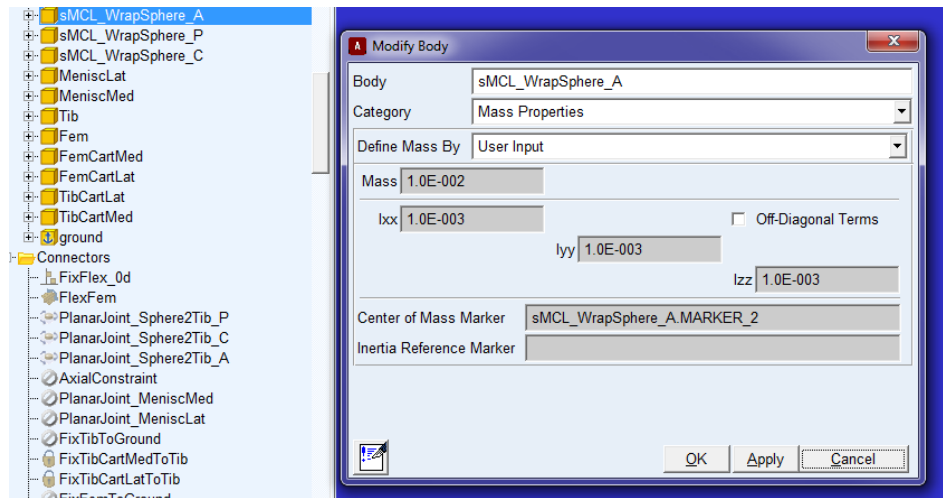

Fig. 53: Mass property for the rigid spheres used in MCL wrapping defined in ADAMS View

3- Define 11 new single-component forces (springs) listed below to restrain the spheres to the proximal tibia (Fig. 54):

    i. **sMCL_WrapDist_A**: connecting the distal tibial insertion of the anterior fiber of   MCL to sphere A

    ii. **sMCL_WrapDist_C**: connecting the distal tibial insertion of the central fiber of   MCL to sphere C

    iii. **sMCL_WrapDist_P**: connecting the distal tibial insertion of the posterior fiber of   MCL to sphere P

    iv. **sMCL_WrapProx_A**: connecting the femoral insertion of the anterior fiber of   MCL to sphere A

    v. **sMCL_WrapProx_C**: connecting the femoral insertion of the central fiber of   MCL to sphere C

<ol start="6" type="i">
sMCL_WrapProx_P: connecting the femoral insertion of the posterior fiber of   MCL to sphere P
sMCL_Sphere2Tib_A: connecting sphere A to the proximal tibia
sMCL_Sphere2Tib_C: connecting sphere C to the proximal tibia
sMCL_Sphere2Tib_P: connecting sphere P to the proximal tibia
sMCL_Sphere2Sphere_A2C: connecting sphere A to sphere C
sMCL_Sphere2Sphere_C2P: connecting sphere C to sphere P
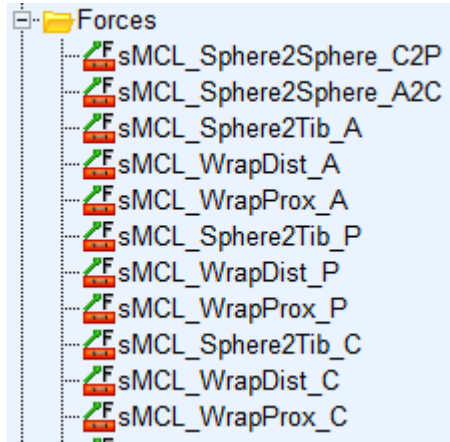

Fig. 54: Springs connecting the three rigid spheres to
each other and to the tibia

The force function for the proximal (3 fibers) and distal (3 fibers) of the sMCL was defined as described in the Ligament Force section of this document.

However, define the force function of the springs between the three spheres (two linear springs) and between the three spheres and the tibia (three linear springs) as follows:

$$F(l, \dot{l}, l_0) = \{[K(l - l_0) + c_d \dot{l} B_1] B_3\} \tag{1a}$$

$$B_1 = step(\dot{l}, 0, 0, \dot{l} + 0.1, 1)$$

$$\tag{1b}$$

$$B_3 = step(l, (l_0 + \varDelta_t), 0, (l_0 + \varDelta_t) + 0.001, 1)$$

Where l is the inter-insertional distance, $\dot{l}$ is the first derivative of the inter-insertional distance with respect to time, and l_0 is the ligament slack length. K is the spring stiffness and was set equal to 5 N/mm for both the sphere-to-bone connection and the sphere-to-sphere connection . The transition between the toe region and linear region is defined by Δ_t. Each force element also included a parallel damping term (c_d = 1.5 Ns/mm) based on the stress relaxation response of ligaments (Funk, Hall et al. 2000). The step functions B_1 and B_3 are cubic polynomials that allow continuous and smooth generation of tensile forces as a ligament fiber becomes taut.

4- Measure the length of each spring and add 9 new design variables (described in section 'Define mass properties, joints, and forces' above) that contain the length of each spring (Fig. 55).

Design Variables
- 123 L0_sMCL_Sphere2Sphere_A2C
- 123 L0_sMCL_Sphere2Sphere_C2P
- 123 L0_sMCL_WrapDist_A
- 123 L0_sMCL_WrapProx_A
- 123 L0_sMCL_WrapDist_P
- 123 L0_sMCL_WrapProx_P
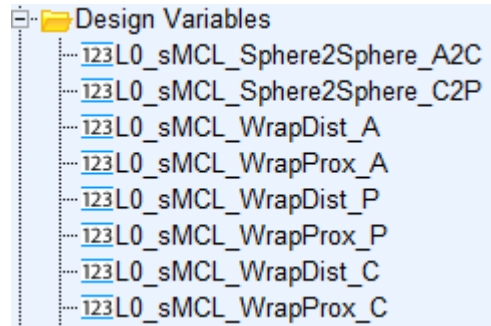- 123 L0_sMCL_WrapDist_C
- 123 L0_sMCL_WrapProx_C

Fig. 55: New design variables that contains the length of
the springs connecting the spheres to the tibia to model
wrapping of the sMCL around the proximal tibia

5- Define three planar joints between the three spheres and the proximal tibia (Fig. 56). The three planar joints are oriented tangent to the proximal tibia and prevent penetration of the spheres into the tibia. The spheres only undergo small translations since they are constrained with springs to the tibia and to each other. If the spheres stay in close proximity to the tibial bone, they retain a physiological line of action of the sMCL around the proximal tibia.
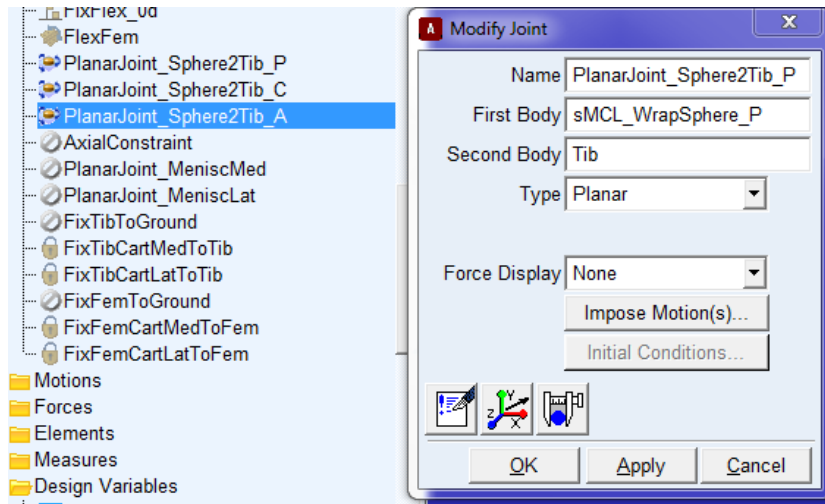
Fig. 56: Planar joint between the spheres and the tibia

Definition of ligament slack length

We used a generalized reduced gradient optimization algorithm to determine the slack lengths (l_0) of the ligament fibers. This optimization included the 29 fibers comprising nine ligaments that, from our observations and cadaveric measurements, were observed to be taut at full extension. The goal of the optimization was to identify l_0 as a percentage of the fiber length at full extension (l_e) in the groups of fibers comprising each ligament (Fig. 57). The objective function described the differences between the resultant ligament forces predicted by the model (F_i^m) and the experimentally-measured ligament forces at full extension (F_i^e) (Eq. 2a). The predicted ligament force was the resultant vectoral magnitude of force in the fibers that comprised each ligament. Altogether, l_0 was optimized for 29 fibers across nine ligaments in this underdetermined system of equations (Eq. 2a). The initial value of l_0 was defined to be the fiber length at full extension, and l_0 was allowed to vary by ±10% from the initial value (Eq. 2b). The optimization was performed with the knee at full extension while permitting the tibia to move in the proximal-distal direction under 10 N of compression. The remaining degrees of freedom were held constant keeping the knee in full extension.

$$\min \sum_{i=1}^{9} \left(\left[\sum_{j=1}^{a} [\vec{F}_{i,j}^{m}(l,\dot{l},l_0)]^2 \right]^{\frac{1}{2}} - F_i^e \right)^4 \tag{2a}$$

a = number of fibers comprising each of the 9 ligaments included in the optimization

$$F_i^m = \{ACL, sMCL, LCL, FFL, OPL, POL, MPC, LPC, PCL_{PM}\}$$
$$F_i^e = \{37, 4, 20, 1, 10, 18, 1, 4, 10\}\ N$$

$$a = \{6\,, 6\,, 1, 1\,, 2\,, 3\,, 3\,, 3\,, 4\} \, fibers$$

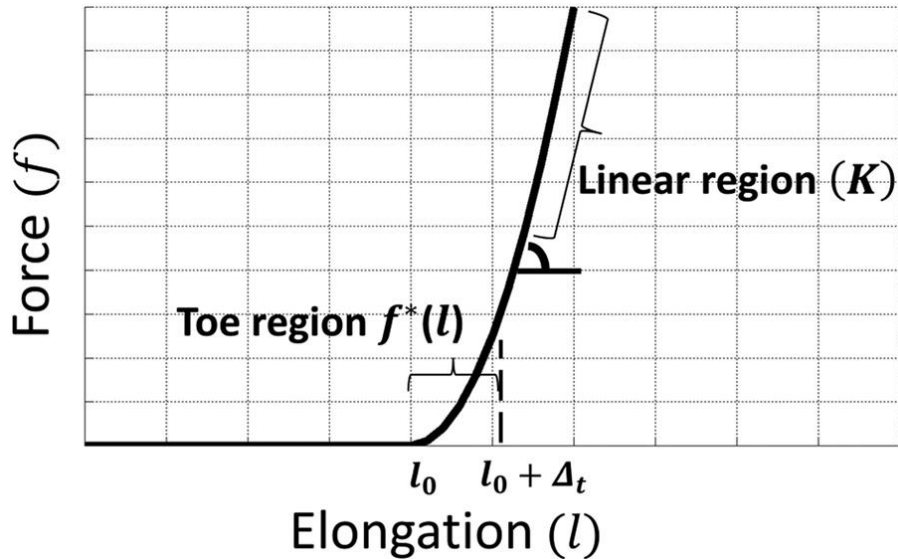$$l_0 = l_e(100 - x)\% \qquad -10 \le x \le +10 \tag{2b}$$

Fig. 57: The force elongation relationship of knee ligaments consisting of slack, toe, and linear regions. Δ_t is the amount of ligament elongation in the toe region

Define the slack length of the ligaments that were observed to be slack (i.e., did not carry force) at full extension and were, therefore, not included in the optimization as follows (Kia, Schafer et al. 2016):

- Define the slack length of the ALL as 115% of its length at full extension based on matching model predictions of the engagement of the ALL to previously-reported experimental data (Thein, Boorman-Padgett et al. 2016). The engagement of the ALL is the resultant force carried by the ALL while the tibia translates anteriorly as an anterior tibial force is increased to 134 N at 30° of flexion.
- Set the slack lengths of the AL fibers of the PCL (PCL_5, PCL_6, PCL_7) to be the percentage defined by their length at full extension and their longest length through at least 120° of passive flexion, which is 110% of their fiber length at full extension. It was previously observed slack at full extension.

70

- Define the slack length of the medial meniscal coronary ligaments (MM_MedMeniscPost, MM_MedMeniscAnt, MM_MedMeniscCent, MM_AntMeniscLat, MM_AntMeniscMed, MM_PostMeniscLat, MM_PostMeniscMed) as 100% of their length at full extension.
- Model the meniscal horns (an anterior and posterior fiber for each meniscus) with a linear, tension-only force–elongation response and stiffness of 180N/mm (no slack or toe regions).

In addition, the six fibers of the posterior capsule (MPC and LPC) became slack at flexion angles >30 deg; thus, deactivate these fibers at flexion angles >30°. To do this, define a state variable (VAR_alpha) with an algebraic function that measure the flexion angle. Add this state variable as part of an IF conditional function at the beginning of the force function of each fiber of the MPC and LPC. The new function looks like this (in bold) (Eq. 3):

if(Varval(.s15_0d_Reference.VAR_alpha)-30:(-(PostCapsule_Stiffness)*(AKISPL (.s15_0d_Reference.Disp_PLC_M,0,SPLINE_sMCL,0))-(Ligs_DampingCoefficient*VR (Eq.3) (Tib_PLC_M,Fem_PLC_M)*Step(VR(Tib_PLC_M,Fem_PLC_M),0,0, VR(Tib_PLC_M,Fem_PLC_M)+0.1,1))) *Step(DM(Tib_PLC_M,Fem_PLC_M),L0_PLC_M,0,L0_PLC_M +0.1,1)**,0,0)**

Optimization steps:

1- Limit the tibiofemoral joint to one proximal-distal degree of freedom along the long axis of the tibia by activating and deactivating the following joints by setting "AxialConstraint" to ON "FixTibToGround" to OFF in ADAMS View.
2- Activate the 10 N compressive force
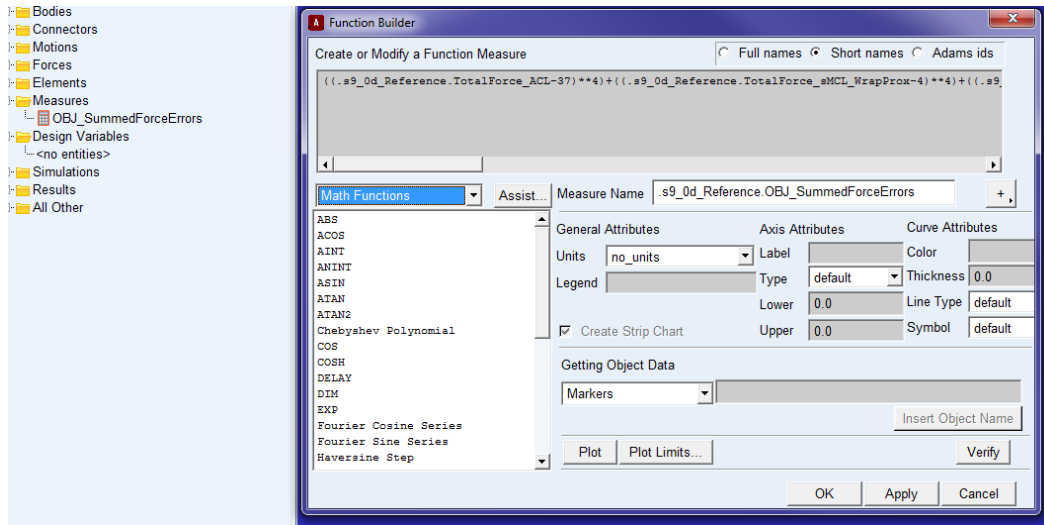3- Create a new measure and call it 'OBJECTIVE_SummedForceErrors' (Fig. 58)

Fig. 58: Objective function definition in ADAMS View

Define the following function in this measure:

((TotalForce_ACL-37)**4) + ((TotalForce_sMCL_WrapProx-4)**4) +

((TotalForce_sMCL_WrapDist-4)**4) + ((Force_LCL-20)**4) + ((.Force_FFL-1)**4) +

((Force_OPL_PL-10)**4) + ((TotalForce_POL-18)**4) + ((TotalForce_PMC-1)**4) +

((TotalForce_PLC-4)**4) + ((TotalForce_PCL_PM-10)**4)

This function represents the sum of the differences between the current ligament forces and the target ligament forces each raised to the fourth power.

4- Define the following constraints: These constraints represent the allowed forces at full extension for each fiber included in the objective function. When running the optimization algorithm, these constraints should not be violated. (Constraint1_PLCForce, Constraint2_PLCForce, Constraint1_PMCForce, Constraint2_PMCForce, Constraint1_FFLForce, Constraint2_FFLForce, Constraint1_OPLForce, Constraint2_OPLForce, Constraint1_ACLForce, Constraint2_ACLForce, Constraint1_LCLForce, Constraint2_LCLForce, Constraint1_POLForce, Constraint2_POLForce, Constraint1_sMCLForces_WrapDist, Constraint2_ sMCLForces_WrapDist, Constraint1_ sMCLForces_Wrapprox, Constraint2_ sMCLForces_Wrapprox, Constraint1_PCLForce, Constraint2_PCLForce)

72

Constraint 1 represents the upper bound of the target ligament pretension, which is the target pretension plus 0.05 N (Fig. 59). Constraint 2 represents the lower bound of this force which is the target ligament pretension minus 0.05 N (Fig. 60).
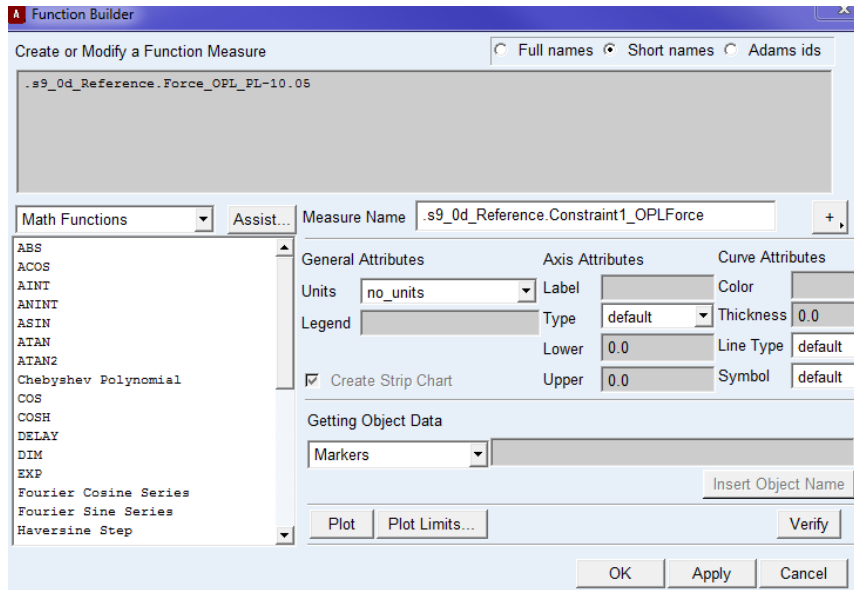

Fig. 59: Sample definition of Constraint 1; in this case applied to the OPL-PL fiber, which is included in the slack length optimization algorithm
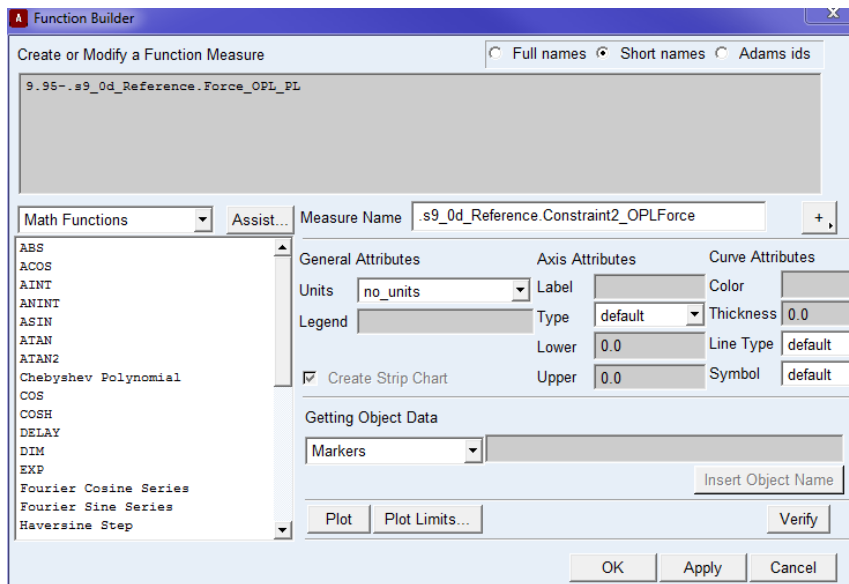

Fig. 60: Sample definition of Constraint 2; in this case applied to the OPL-PL fiber, which is included in the slack length optimization algorithm

5- Click the 'Design Evaluation Tools' in ADAMS View (Fig. 61)

6- Right-click in the 'Simulation Script' bar, and choose 'LigL0_OptimizationScript'.

7- Choose 'Study a: Objective'

8- Right-click in the objective bar, and select 'OBJECTIVE_SummedForceErrors'

9- Select "Optimization"

10- Right Click in Design Variables and select:
(Percent_L0_AnteriorCruciates, Percent_L0_FFL, Percent_L0_LCL, Percent_L0_sMCL, Percent_L0_POL, Percent_L0_OPL, Percent_L0_PMC, Percent_L0_PLC)

11- Goal: Minimize Design Measure/Objective

12- Check the 'Constraints' box, right click in the box, and select all constraints of ligament forces described in step 4.
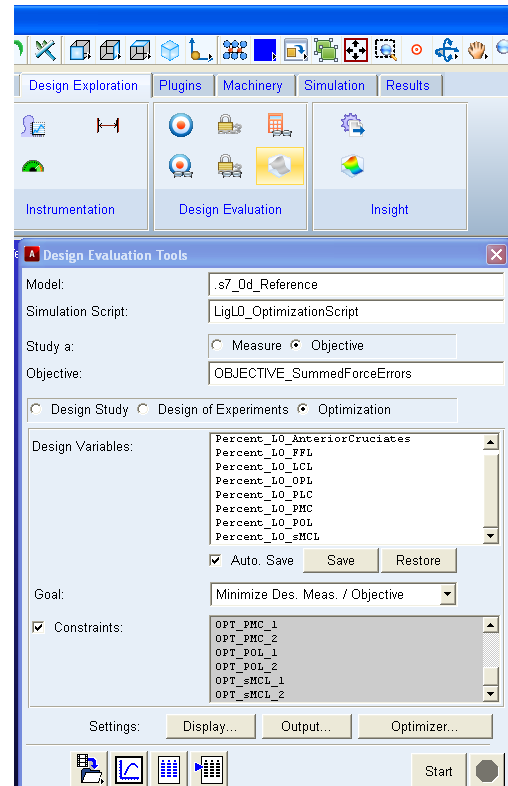
13- Select 'Start'.

Fig. 61: Design evaluation settings used to define the slack length optimization problem for selected ligaments that are taut at full extension in ADAMS View

NOTE: Manually reduce the design variables by a percent or two before running this optimization; e.g.: Change 'Percent_L0_sMCL from 1.0→0.985. Doing so can reduce optimization time, and reduces the chance that the optimization will fail (i.e., not find a solution). If the optimization still fails, manually adjust the design variables further from 0.985 to 0.975 to get closer to the solution.

Passive flexion

To passively flex the knee, define the following joints, motions, and forces:

a) Define a revolute joint (Fig. 62) between the femur and the ground aligned with the transepicondylar axis (Y-axis) of the femur (location: 0,0,0; orientation: -90,0,90). This joint limits the femur to one degree of freedom.
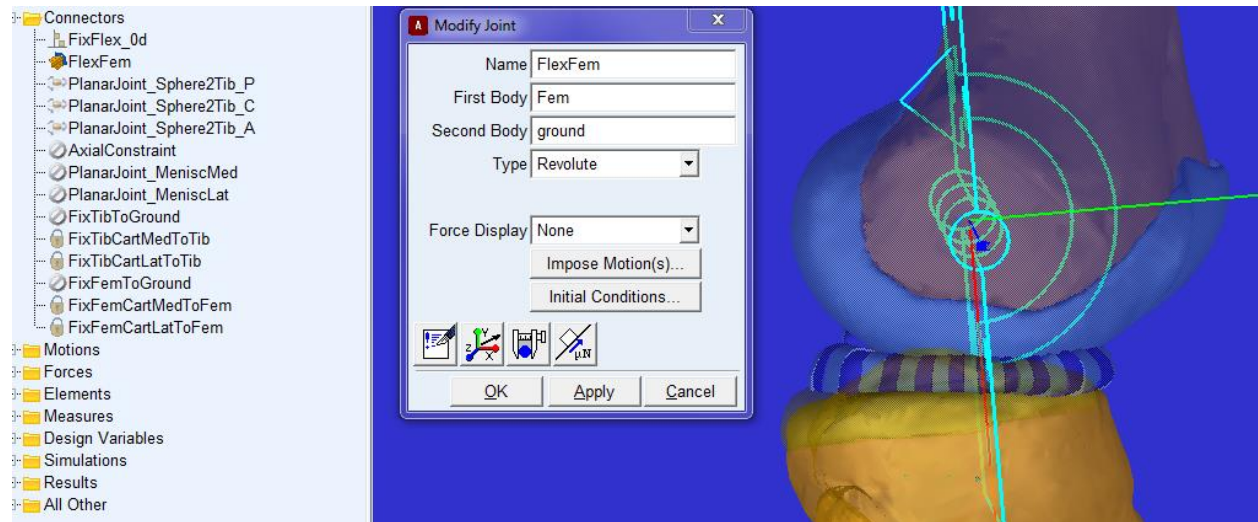

Fig. 62: Definition of the flexion-extension revolute joint between the femur and the ground

b) Define a Joint Motion to the revolute joint. That is, rotate the femur in flexion about the transepicondylar (Y-axis) axis (Fig. 63).
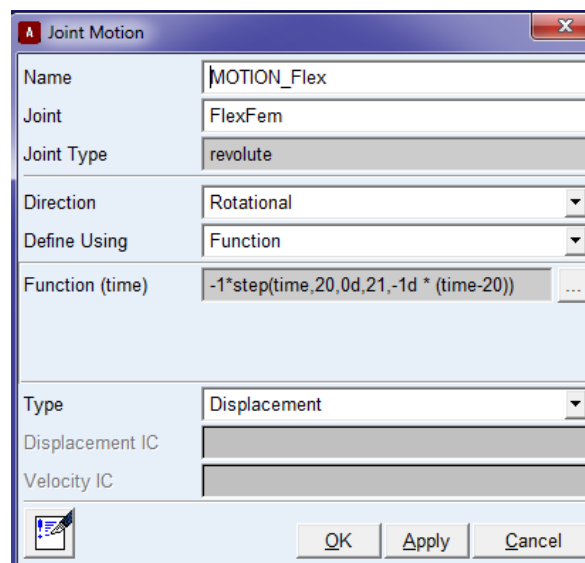

Fig. 63: Definition of the flexion motion

c) Create a measure for the revolute joint to calculate the flexion angle (Fig. 64).
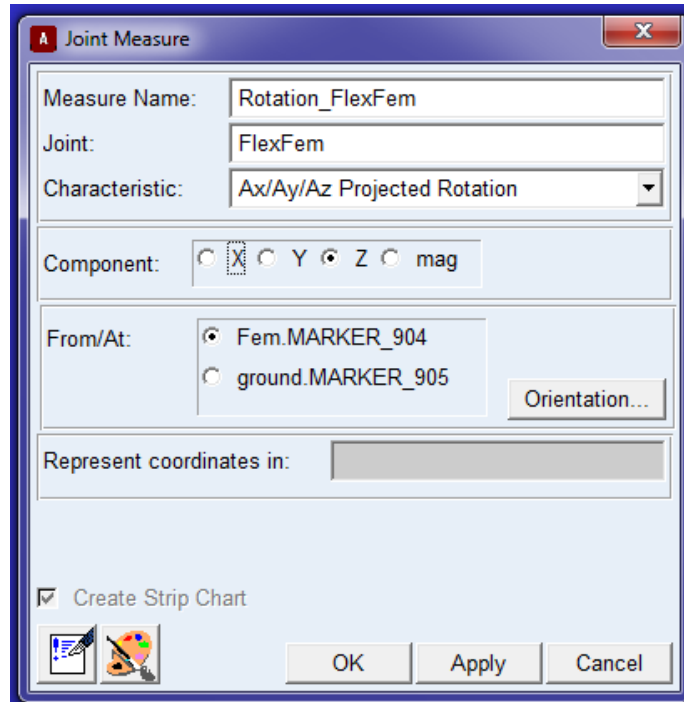

Fig. 64: Creating a measure of the flexion angle

d) Define a perpendicular primitive joint between the tibia and the ground (Fig. 65). This allows the tibia five degrees of freedom except for the direction of flexion/extension. Since the femur has one degree of freedom (in flexion/extension) and the tibia has five degrees of freedom, the knee joint has six degrees of freedom.
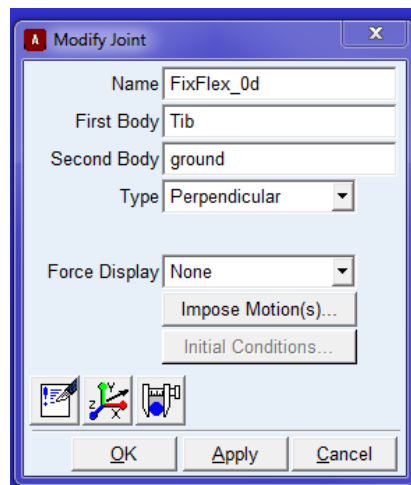

Fig. 65: A primitive joint between the tibia and the ground to lock flexion/extension of the tibia

e) Deactivate the axial constraint between femur and tibia.

f) Apply 10 N of compression to the knee along the long axis of the tibia (Fig. 66). This reflects what our laboratory commonly does during cadaveric studies (Imhauser, Mauro et al. 2013).
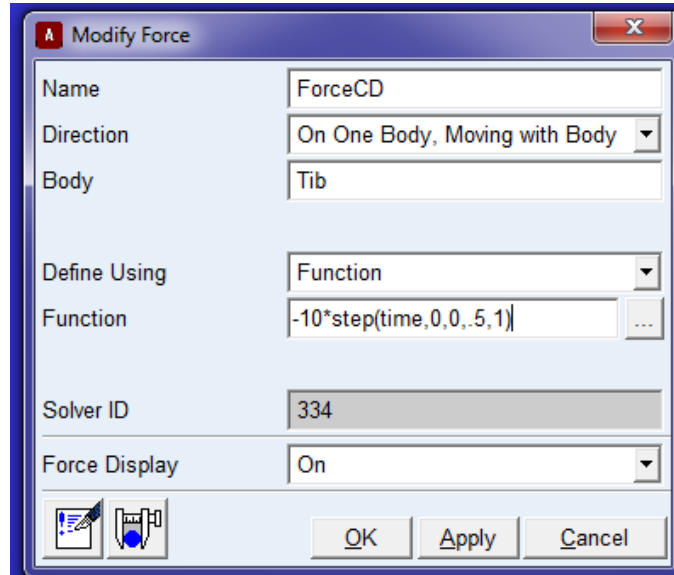
Fig. 66: Applying a compressive load to the knee along the long axis of the tibia

g) Deactivate the fixed joint between the femur and the ground

h) Modify the forces of the lateral and medial posterior capsule so that they deactivate at ≥30° of flexion: PLC_L, PLC_C, PLC_M, PMC_L, PMC_C, PMC_M

i) Run the simulation for 101 seconds to achieve 100° of flexion using the simulation parameters defined in the Numerical analysis section.

References

Amirtharaj, M. J., B. Hardy, et al. (2018). "Automated, Accurate, and Three-dimensional Method for Calculating Sagittal Slope of the Tibial Plateau." Journal of biomechanics.

Amis, A., P. Firer, et al. (2003). "Anatomy and biomechanics of the medial patellofemoral ligament." The Knee **10**(3): 215-220.

Basso, O., D. Johnson, et al. (2001). "The anatomy of the patellar tendon." Knee Surgery, Sports Traumatology, Arthroscopy **9**(1): 2-5.

Beidokhti, H. N., D. Janssen, et al. (2017). "The influence of ligament modelling strategies on the predictive capability of finite element models of the human knee joint." Journal of biomechanics **65**: 1-11.

Blankevoort, L. and R. Huiskes (1996). "Validation of a three-dimensional model of the knee." Journal of biomechanics **29**(7): 955-961.

Butler, D. L., Y. Guan, et al. (1992). "Location-dependent variations in the material properties of the anterior cruciate ligament." Journal of biomechanics **25**(5): 511-518.

Claes, S., E. Vereecke, et al. (2013). "Anatomy of the anterolateral ligament of the knee." Journal of anatomy **223**(4): 321-328.

Criscenti, G., C. De Maria, et al. (2016). "Material and structural tensile properties of the human medial patello-femoral ligament." Journal of the mechanical behavior of biomedical materials **54**: 141-148.

De Maeseneer, M., P. Van Roy, et al. (2004). "Normal anatomy and pathology of the posterior capsular area of the knee: findings in cadaveric specimens and in patients." AJR. American journal of roentgenology **182**(4): 955-962.

Funk, J., G. Hall, et al. (2000). "Linear and quasi-linear viscoelastic characterization of ankle ligaments." Journal of Biomechanical Engineering **122**(1): 15-22.

Galante, J., W. Rostoker, et al. (1970). "Physical properties of trabecular bone." Calcified tissue research **5**(3): 236-246.

Gear, C. W. (1971). "Simultaneous numerical solutionof differential algebraic equations." <u>IEEE Trans Circuit Theory</u> **18**: 89-95.

Giffin, J. R., M. J. Haemmerle, et al. (2002). "Single- versus double-bundle PCL reconstruction: a biomechanical analysis." <u>The journal of knee surgery</u> **15**(2): 114-120.

Grood, E. S. and W. J. Suntay (1983). "A joint coordinate system for the clinical description of three-dimensional motions: application to the knee." <u>Journal of Biomechanical Engineering</u> **105**(2): 136-144.

Guess, T. M., G. Thiagarajan, et al. (2010). "A subject specific multibody model of the knee with menisci." <u>Medical engineering & physics</u> **32**(5): 505-515.

Hara, K., T. Mochizuki, et al. (2009). "Anatomy of normal human anterior cruciate ligament attachments evaluated by divided small bundles." <u>The American journal of sports medicine</u> **37**(12): 2386-2391.

Harner, C. D., J. W. Xerogeanes, et al. (1995). "The human posterior cruciate ligament complex: an interdisciplinary study: ligament morphology and biomechanical evaluation." <u>The American journal of sports medicine</u> **23**(6): 736-745.

Hauch, K. N., D. F. Villegas, et al. (2010). "Geometry, time-dependent and failure properties of human meniscal attachments." <u>Journal of biomechanics</u> **43**(3): 463-468.

Haut, T. L. and R. C. Haut (1997). "The state of tissue hydration determines the strain-rate-sensitive stiffness of human patellar tendon." <u>Journal of biomechanics</u> **30**(1): 79-81.

Hutchinson, M. R. and S. A. Ash (2003). "Resident's ridge: assessing the cortical thickness of the lateral wall and roof of the intercondylar notch." <u>Arthroscopy : the journal of arthroscopic & related surgery : official publication of the Arthroscopy Association of North America and the International Arthroscopy Association</u> **19**(9): 931-935.

Imhauser, C., C. Mauro, et al. (2013). "Abnormal tibiofemoral contact stress and its association with altered kinematics after center-center anterior cruciate ligament reconstruction: an in vitro study." <u>The American journal of sports medicine</u> **41**(4): 815-825.

Imhauser, C. W. (2004). "Development and evaluation of a 3-dimensional, image-based, patient-specific, dynamic model of the hindfoot (The)."

Imhauser, C. W., S. Siegler, et al. (2008). "Subject-specific models of the hindfoot reveal a relationship between morphology and passive mechanical properties." Journal of biomechanics **41**(6): 1341-1349.

Kennedy, M. I., S. Claes, et al. (2015). "The anterolateral ligament: an anatomic, radiographic, and biomechanical analysis." The American journal of sports medicine **43**(7): 1606-1615.

Kia, M., K. Schafer, et al. (2016). "A multibody knee model corroborates subject-specific experimental measurements of low ligament forces and kinematic coupling during passive flexion." Journal of Biomechanical Engineering **138**(5): 051010.

Kia, M., A. P. Stylianou, et al. (2014). "Evaluation of a musculoskeletal model with prosthetic knee through six experimental gait trials." Medical engineering & physics **36**(3): 335-344.

LaPrade, R. F., A. H. Engebretsen, et al. (2007). "The anatomy of the medial part of the knee." The Journal of bone and joint surgery. American volume **89**(9): 2000-2010.

LaPrade, R. F., T. V. Ly, et al. (2007). "The anatomy of the medial part of the knee." JBJS **89**(9): 2000-2010.

LaPrade, R. F., T. V. Ly, et al. (2003). "The posterolateral attachments of the knee." The American journal of sports medicine **31**(6): 854-860.

LaPrade, R. F., P. M. Morgan, et al. (2007). "The anatomy of the posterior aspect of the knee. An anatomic study." The Journal of bone and joint surgery. American volume **89**(4): 758-764.

Lasdon, L. S., R. J. Fox, et al. (1974). "Nonlinear optimization using the generalized reduced gradient method." RAIRO - Operations Research - Recherche Opérationnelle **3**(8): 73-103.

Liu, F., B. Yue, et al. (2010). "Morphology of the medial collateral ligament of the knee." Journal of orthopaedic surgery and research **5**(1): 1.

Lopes Jr, O. V., M. Ferretti, et al. (2008). "Topography of the femoral attachment of the posterior cruciate ligament." <u>JBJS</u> **90**(2): 249-255.

Materialise, T. (2013). Mimics 17.0 Reference Guide. Materialise**:** 575.

Merican, A. M., S. Sanghavi, et al. (2009). "The structural properties of the lateral retinaculum and capsular complex of the knee." <u>Journal of biomechanics</u> **42**(14): 2323-2329.

Mochizuki, T., H. Fujishiro, et al. (2014). "Anatomic and histologic analysis of the mid-substance and fan-like extension fibres of the anterior cruciate ligament during knee motion, with special reference to the femoral attachment." <u>Knee surgery, sports traumatology, arthroscopy : official journal of the ESSKA</u> **22**(2): 336-344.

MSCsoftware, A. t. a. (2012). Adams Tutorial Kit for Mechanical Engineering Courses (second edition). M. software**:** 309.

Quapp, K. and J. Weiss (1998). "Material characterization of human medial collateral ligament." <u>Journal of Biomechanical Engineering</u> **120**(6): 757-763.

Robinson, J. R., A. M. Bull, et al. (2005). "Structural properties of the medial collateral ligament complex of the human knee." <u>Journal of biomechanics</u> **38**(5): 1067-1074.

Sasaki, N., Y. Ishibashi, et al. (2012). "The femoral insertion of the anterior cruciate ligament: discrepancy between macroscopic and histological observations." <u>Arthroscopy : the journal of arthroscopic & related surgery : official publication of the Arthroscopy Association of North America and the International Arthroscopy Association</u> **28**(8): 1135-1146.

Tajima, G., M. Nozaki, et al. (2009). "Morphology of the tibial insertion of the posterior cruciate ligament." <u>JBJS</u> **91**(4): 859-866.

Thein, R., J. Boorman-Padgett, et al. (2016). "Biomechanical assessment of the anterolateral ligament of the knee: a secondary restraint in simulated tests of the pivot shift and of anterior stability." <u>JBJS</u> **98**(11): 937-943.

Tsukada, S., H. Fujishiro, et al. (2014). "Anatomic variations of the lateral intercondylar ridge: relationship to the anterior margin of

the anterior cruciate ligament." <u>The American journal of sports medicine</u> **42**(5): 1110-1117.

Vincent, J.-P., R. A. Magnussen, et al. (2012). "The anterolateral ligament of the human knee: an anatomic and histologic study." <u>Knee Surgery, Sports Traumatology, Arthroscopy</u> **20**(1): 147-152.

Wilson, W. T., A. H. Deakin, et al. (2012). "Comparative analysis of the structural properties of the collateral ligaments of the human knee." <u>The Journal of orthopaedic and sports physical therapy</u> **42**(4): 345-351.

Ziegler, C. G., S. D. Pietrini, et al. (2011). "Arthroscopically pertinent landmarks for tunnel positioning in single-bundle and double-bundle anterior cruciate ligament reconstructions." <u>The American journal of sports medicine</u> **39**(4): 743-752.